Experimental study on the effect of the ventilation and operation mode on the thermal efficiency of a full-scale Trombe wall under real operating conditions

Solar Energy 302 (2025) 114039

Contents lists available at ScienceDirect

Solar Energy

journal homepage: www.elsevier.com/locate/solener

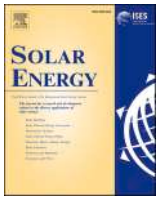

Experimental study on the effect of the ventilation and operation mode on the thermal efficiency of a full-scale Trombe wall under real operating conditions

Aikaterina Karanafti [a,*], Elena Badino [b], Valentina Serra [b], Stefano Fantucci [b]

[a] Laboratory of Building Construction and Building Physics, Civil Engineering Department, Aristotle University of Thessaloniki, PO BOX 429, 54124 Thessaloniki, Greece
[b] TEBE Research Group, Department of Energy, Politecnico di Torino, Corso Duca degli Abruzzi 24, 10129 Torino, Italy

ARTICLE INFO

Keywords:
Trombe wall
Solar wall
Opaque double skin facade
Indoor air curtain
Supply air façade

ABSTRACT

Improving energy efficiency and occupant comfort in buildings is essential for reducing resource use and emissions. Trombe walls help achieve this by lowering heating demand through solar gains, though further research is needed to fully harness their potential. This study presents an experimental campaign carried out in winter on three parallel full-scale fan-assisted Trombe wall modules installed in an existing residential building in Turin, northern Italy. The three modules are characterized by different operating modes: a Thermal Buffer (TB) mode (closed cavity), an Indoor Air Curtain (IAC) mode, and a Supply Air Façade (SAF) mode (pre-heating outdoor air). The last two modes make use of a fan, providing a supply air flow rate of approximately 43 m^3/h. An in-depth comparative analysis of the modules' performance and heating efficiency was conducted. The results demonstrate that these systems can be considered sustainable and efficient strategies, pointing out the systems' ability to effectively heat the air in the cavity in all three operation modes. Indeed, the air in the cavity reaches temperatures between 50 °C and 60 °C in the IAC and the SAF modes, and over 60 °C in the TB mode, while the air entering the building is mostly beyond 30 °C during the fan operation. For the IAC mode, system's total efficiencies (accounting for gains from heated air and the massive wall) were reported as 12.6 % with partial façade shading and 18.4 % with no shading, while for the SAF mode, the relevant efficiency reaches 15.6 % with partial shading and 23.7 % with no shading.

1. Introduction

Highly efficient building envelopes are an essential component of nearly zero-emission buildings (NZEBs) and zero-emission buildings (ZEBs) since they affect the buildings' overall performance to a great extent. Proper retrofitting of the existing building stock can significantly mitigate global energy consumption and emissions, mitigating at the same time the climate change effects. It is reported that since 2015 energy efficient interventions in building envelopes decreased by 7 % the heating intensity [1].

In the last decades, various building envelope systems exhibiting different complexity levels have been tested for their potential contribution to the buildings' performance enhancement. The increasing buildings' energy demand combined with the need for energy mitigation, contributed to the development of innovative envelope technologies with more advanced performance than the conventional ones. Ventilated facades [2], dynamic insulation systems [3], double skin façade (DSF) [4], and adaptive facades [5], maximize the benefits of the prevailing climatic conditions, in contrast with conventional insulation systems which merely isolate the indoor environment from the outdoor one.

Passive solar systems take advantage of solar radiation to mainly heat the indoor environment [6]. Trombe wall (TW) is a notable example of this approach [7]. Numerous studies have been published over the years to explore and document the full range of the potential benefits a building can acquire from a TW's installation. Since the initial development of the TW system, several modifications of its configuration have been released, all of which aim to effectively address one or more of its weak points. Although there are many experimental TW studies, some aspects still remain unexplored.

* Corresponding author.
E-mail address: akaranaf@civil.auth.gr (A. Karanafti).

https://doi.org/10.1016/j.solener.2025.114039
Received 11 April 2025; Received in revised form 14 July 2025; Accepted 3 October 2025
Available online 13 October 2025

1.1. State-of-the-art and research gap

The classical TW was firstly introduced back in 1881 by the American engineer Edward Morse [8], while it was named after Felix Trombe and Jacque Michel many decades later when they implemented it in a building [9]. It consists of a massive storage wall, an air cavity, and an external glazing. Usually, vents are installed to enhance the convection effect and consequently, the overall system's performance. The incident solar radiation heats the storage wall, while the external glazing contributes to the development of the greenhouse effect in the cavity. The wall then dissipates the stored heat in the indoor environment, a phenomenon that can be further enhanced by parallel air circulation through the vents. The main challenges of this approach are mainly related to the lack of insulation and the low thermal resistance of the component, which make the wall vulnerable to outdoor conditions. Specifically, during nighttime or cloudy weather, the low thermal resistance of the wall is strongly related to potential temperature fluctuations of the storage wall, and may also cause reversed airflow in the cavity if the vents remain constantly open [7]. The aesthetic aspect is also a matter of great concern, as the surface of the massive wall facing the cavity is usually painted black to increase solar absorption, potentially making the architectural integration of these systems challenging.

To properly address the aforementioned challenges, some of which vary among the different climates, a precise analysis of the TW is required. One of the most important factors that affect both the heat absorption and the heat losses from the wall is the glazing type. There is no norm defining the optimum solution for the glazing type, as the results of the existing studies vary among different regions [9]. Design parameters like the aspect ratio (cavity width/cavity height) and the ventilation type (natural or forced) need to be also thoroughly examined, as they affect the system's efficiency [10]. Moreover, the implementation of fins in a classical TW seems to improve the performance, especially in cases with medium solar radiation levels [11,12].

Throughout the years various modifications in the classical TW, either in the design approach or with the addition of advanced materials, have been investigated. Some studies have tried to categorize TW configurations based on their features. Among the studies classifying the existing TW configurations most of the categories are common, whilst few differentiations can be detected. Hu et al. classified the existing systems into different categories, namely the classical, the composite, the water, the zigzag, the *trans*-wall, the fluidized, and the photovoltaic (PV) TW [9]. Saadatian et al. added two extra categories, that of the Phase Change Material (PCM) and the hybrid TW [8]. On the other hand, Wang et al. excluded the hybrid and zigzag TW categories and added the air-purification and electrochromic TW ones [13].

To make things clear, a brief description of each TW type is provided in Table 1.

Numerous studies, experimental and simulation-based, have been published in the last few years, focusing on the examination of all the TW categories. In Table 2 the most recent in-field experimental studies were gathered, considering those published from 2010 on, until March 2025. Details about the climatic conditions, the ventilation mode, the glazing type, the storage wall type, the monitoring period, and the experimental apparatus used are presented. Regarding the experimental apparatus classification, the categories presented in [12] were adopted with a few modifications. In particular, the apparatus used is divided into "reduced-scale test rooms", "full-scale test rooms", "stand-alone TW modules", and "actual testing houses". In the last category, a further clarification was made when the testing building was occupied. An arbitrary threshold separating the "reduced-scale" and the "full-scale" thermal room was set at the 2 m height of the test cell. So, test cells of height lower or equal to 2 m were considered reduced-scale, otherwise, they were classified as full-scale.

It is evident that the majority of the studies focus on classical TW assemblies, with the PV TWs gathering the second biggest portion of the research. Other types, like the PCM TWs, the composite, and the water

Table 1
Brief description of the existing TW configurations and their main difference with the classical TW.

TW type	Main differentiation from classical TW	Reference
Composite TW/ Trombe-Michel wall	Existence of an unventilated cavity between the glazing unit and the massive wall. The ventilated cavity is placed behind the massive wall. An insulation layer separates the ventilated cavity from the indoor environment.	[14]
Water TW	Same working principle. Using water as heat storage medium.	[15]
Zigzag TW	It consists of 3 sections: one faces south, the others form a V-shape. Two sections have the form of a classical TW, while the southeast consists of a window taking advantage of the early morning solar gains.	[8,16]
Trans-wall	Consists of transparent containers filled with water having absorbers between them to collect solar heat and transfer it to the water.	[17,18]
Fluidized TW	The cavity is filled with low density particles with high absorptivity to heat more effectively the circulating air.	[19]
PV TW	The solar cells implemented in a classical TW contribute to electricity production.	[20]
PCM TW	Making use of PCM's latent heat storage capacity to enhance a TW's efficiency.	[21]
Hybrid TW	Acting as a classical TW during the heating season, it can adapt its function during the cooling period. A blind can be rolled down to prevent heat gains, while the implementation of a porous ceramic which can absorb water is used when needed to cool the air.	[8,22]
Air-purification TW	Through a catalytic reaction, formaldehyde pollutants are degraded into H_2O and CO_2. This TW function operates in parallel with its main heating function.	[23]
Electrochromic TW	Existence of an electrochromic glazing instead of a normal glazing, which can adjust its properties between winter and summer.	[24]

TWs have not been studied in the field to a great extent yet. Water and PCMs in a TW actually replace the massive storage wall and act as storage mediums. In fact, PCMs present the advantage of combining a high heat storage capacity together with a light weight, and the selection of the proper PCM type should be mainly based on the solar radiation intensity in the examined area [85].

Apart from the TW categories defined in the literature review studies, five extra TW types were identified in the most recent studies. One of the extra configurations combines the beneficial effect of PCMs with a PV panel [56], while the second refers to a PV TW which purifies also the supplied air [26,37]. A TW operating as a thermal diode was also examined experimentally in [54]. Finally, PCMs combination with radiation refrigeration [31], and air purification [32], in advanced TW assemblies presented significant advantages in recent studies.

TWs are mainly passive solar heating systems. Nevertheless, under certain design conditions, they can act also as passive solar cooling systems. This TW ability was investigated in a few studies, as it can be easily observed from the limited number of studies covering the summer period collected in Table 2.

Focusing on the classical TW studies, it can be stated that more than 80 % of the examined walls operate with natural ventilation, while only 12 % make use of mechanical ventilation. The rest 8 % of the studies examined a TB mode of the TW or created a vacuum gap between the absorber and the glass. Moreover, the monitoring period of the systems' performance in most studies consists of only a few days in specific seasons. Apart from this, a limited number of studies have examined the behavior of a classical TW operating under forced ventilation. Only one

Table 2
Summary of the experimental in-field studies of TWs from 2010 and on.

Study	Climate	Year	TW type	Ventilation	Glazing	Storage Wall	Experimental apparatus	Monitoring period
[16]	Wuhan, China	2024	ZTW[a]	Natural	Double glazing Low-E	Heavyweight	RSTR[o]	1 day in January
[15]	Hefei, China	2023	WTW[b]	Natural	NCS[n]	Lightweight	FSTR[p]	10 months (March-December)
[25]	Hefei, China	2022	APTW[c]	Natural	Borosilicate glass	–	SATWM[q]	1 day in November
[26]	Hefei, China	2020	PVAPTW[d]	Natural	Low-iron glass	–	FSTR	6 days in December
[20]	Hefei, China	2019	PVTW[e]	Natural	Clear-single	Heavyweight	FSTR	3 days in December
[27]	Hefei, China	2017	APTW	Natural	Clear-single	–	SATWM	1 day in February
[28]	Hefei, China	2015	CTW[f]	Natural	Clear-single	Heavyweight	FSTR	3 days in January
[29]	Hefei, China	2011	PVTW	Natural	Clear-single & PV panel	NCS	FSTR	Winter
[30]	Sichuan, China	2023	CTW	Natural	Organic	Lightweight	RSTR	2 days in January
[23]	Nanjing, China	2023	APTW	Natural & Forced	Clear-single	–	SATWM	3 days in November
[31]	Nanjing, China	2024	RC-PCMTW[g]	Natural	Clear	Heavyweight	RSTB	Late July to mid-September
[32]	Nanjing, China	2024	PCMAPTW[h]	Natural	NCS	Heavyweight	RSTB	2 days in November
[33]	Nanjing, China	2024	PVTW	Natural	PV panel	NCS	FSTB	~20 days May to June
[34]	Nanjing, China	2025	APTW	Natural	NCS	Lightweight	RSTB	~8 h of a day in March
[21,35]	Yuzhong, China	2020, 2021	PCMTW[i]	Natural	Clear-single	Heavyweight	ATH-OC[r]	16 days in March
[36]	Dongguan, China	2022	PCMTW	Natural	Clear-double	Lightweight	RSTR	4 days in July
[37]	Xining, China	2022	PVAPTW	Natural	Low-iron glass	Heavyweight	FSTR	1 day in October
[38]	Xining, China	2021	APTW	Natural	Clear-single	–	FSTR	1 day in October
[39]	Shihezi, China	2021	CTW	Natural	Clear-double	Heavyweight	ATH[s]	December to January
[14]	Qingdao, China	2021	CoTW[j]	Forced	Clear-single	Heavyweight	FSTR	1 day in January
[40]	Xiangtan, China	2019	CTW	Natural	Glass curtain wall	Lightweight	FSTR	August
[41]	Xiangtan, China	2018	CTW	Natural	Clear	Lightweight	FSTR	July & August
[42]	Harbin, China	2019	CTW	Natural	Clear-double	Lightweight	FSTR	6 days in March
[43]	Haidong, China	2018	CTW	Natural	Glass coated with absorbing layer	NCS	ATH-OC	January
[44]	GangCha, China	2013	CTW	Natural	Clear-single	Heavyweight	FSTR	NCS
[45,46,47]	Borj Cedria, Tunisia	2016, 2017, 2015	CTW	Natural	NCS	Heavyweight	RSTR	NCS
[48]	Kalnciems, Latvia	2023	CTW	Forced	Polycarbonate	Lightweight	ATH-OC	Spring-Autumn
[49]	Izmir, Turkey	2012	CTW & PVTW	Natural	Clear-single/double, Semi-transparent PV panel	Heavyweight	FSTR	2 days in February
[50]	Izmir, Turkey	2013	PVTW	Natural	PV panel	Heavyweight	FSTR	January to April
[51]	Erzerum, Turkey	2012	PCMTW	Forced	Special triple glazing	Heavyweight	FSTR	1 year
[52]	Usak, Turkey	2025	CTW	Natural	NCS	Lightweight	RSTB	1 day in June
[53]	Rzeszów, Poland	2021	CTW	TBM[m]	Clear-double	Heavyweight	FSTB	1 year
[54]	Rzeszów, Poland	2020	TDTW[k]	Natural	Clear-single	–	FSTR	December to March
[55]	Hawija, Iraq	2022	PVTW	Forced	PV panel	Lightweight	RSTR	4 days in October
[56]	Hawija, Iraq	2022	PCMPVTW[l]	Forced	PV panel	Lightweight	RSTR	10 days between August and September
[57]	Hawija, Iraq	2022	PVTW	Natural & Forced	PV panel	Lightweight	RSTR	4 days in April
[58]	Hawija, Iraq	2022	PVTW	Forced	PV panel	Lightweight	RSTR	August to October
[59]	Kirkuk, Iraq	2022	PVTW	Forced	Clear-single & PV panel	Heavyweight	RSTR	December to February
[60]	Kirkuk, Iraq	2021	PVTW	Forced	Clear-single & PV panel	Lightweight	RSTR	April to June
[61]	Kirkuk, Iraq	2020	PVTW	Forced	Clear-single & PV panel	Lightweight	RSTR	April & May
[62]	Kirkuk, Iraq	2024	CTW	Vacuum cavity	Transparent acrylic	Heavyweight	SATWM	4 days in spring
[63]	Kirkuk, Iraq	2024	CoTW	Natural	Transparent acrylic	Heavyweight	FSTB	December to March
[64,65]	Yazd, Iran	2015, 2019	CTW	Natural	Clear	Heavyweight	FSTR	January, February
[66]	Abha, Saudi Arabia	2022	CTW	Natural	Clear-single	Lightweight	FSTR	December
[67]	Abha, Saudi Arabia	2022	PVTW	Forced	PV panel	Heavyweight	FSTR	February to July
[68]	Abha, Saudi Arabia	2021	PVTW	Natural	PV panel	NCS	RSTR	March to July
[69]	Batna, Algeria	2022	CTW	Natural	Clear	Heavyweight	FSTR	typical winter days
[70]	Kitakyushu, Japan	2022	CoTW	Forced	Clear-single	Heavyweight	FSTR	13 days in January
[71,72,73]	Vila Real, Portugal	2021, 2017, 2017	CTW	Natural	Clear-double	Heavyweight	FSTR	August to November
[74]	Coimbra, Portugal	2020	WTW	Natural	Double	Lightweight	FSTR	July to January

(*continued on next page*)

Table 2 (*continued*)

Study	Climate	Year	TW type	Ventilation	Glazing	Storage Wall	Experimental apparatus	Monitoring period
[75]	Madrid, Spain	2021	CTW	Forced	Laminated yellow-tainted	Heavyweight	FSTR	December to September
[76]	Coronel, Chillan, Chile	2020	WTW	Natural & Forced	Clear-single	Lightweight	FSTR	1 year
[77]	Sinai, Egypt	2019	CTW	Natural	Double-high reflective	Heavyweight	ATH-OC	1 year
[78]	Sohag, Egypt	2024	CTW	Natural	Clear-single	Heavyweight	FSTB	Specific days in all summer months from 8a.m. to 6p.m.
[79]	Bangkok, Thailand	2017	CTW	Natural	–	Heavyweight	ATH	1 year
[80]	Curitiba, Brazil	2013	CTW	Natural	Clear-double	Heavyweight	FSTR	Cold periods of 2011 and summer of 2012
[81]	Bethune, France	2012	CoTW	Natural	Clear-double	Lightweight	RSTR	2 weeks April to May
[82,83]	Ancona, Italy	2012	CTW	Natural	Clear	Heavyweight	ATH-OC	2 summers/1 year
[84]	Turin, Italy	2018	CTW	Forced & TBM	Clear-single & Polycarbonate panel	Lightweight	RSTR & FSTR	NCS

[a]ZTW: Zigzag TW
[b]WTW: Water TW
[c]APTW: Air purification TW
[d]PVAPTW: Photovoltaic air purification TW
[e]PVTW: Photovoltaic TW
[f]CTW: Classical TW
[g]RC-PCMTW: Radiation refrigeration PCM TW
[h]PCMAPTW: PCM air purification TW
[i]PCMTW: Phase Change Material TW
[j]CoTW: Composite TW
[k]TDTW: Thermal diode TW
[l]PCMPVTW: Phase Change Material photovoltaic TW
[m]TBM: Thermal buffer mode
[n]NCS: Not clearly stated
[o]RSTR: Reduced-scale test room
[p]FSTR: Full-scale test room
[q]SATWM: Stand-alone TW module
[r]ATH-OC: Actual testing house – occupied
[s]ATH: Actual testing house

study exists in an actual testing house which is occupied at the same time [48]. This unique study is focused on a factory building with a lightweight envelope. It is evident that there is a lack of in-field experimental studies examining the performance of a classical TW with a massive storage wall and mechanical ventilation implemented in an actual testing house.

1.2. Novelty & contribution of the current study

To address the already mentioned research gap, this paper presents the results of an experimental study on a classical TW installed in a residential building in Turin, Italy. The TW operates with forced ventilation and consists of a heavyweight massive storage wall, providing useful input on the effectiveness of this TW type under actual operating conditions. To effectively manage and control ventilation, a fan-assisted TW typology was selected. The adoption of an active ventilation system led to the downsizing of the vents dimensions which consequently reduces the night-time heat losses, which is a major drawback of TWs, as vent area constitute the weakest point of a TW, usually characterized by low airtightness and thermal resistance. The thermal behavior of the TW was monitored for the entire winter period, allowing to investigate the wall's contribution to the heating of the indoor space, in contrast with most of the existing experimental studies which refer to a short monitoring period of a few days or weeks. Moreover, in the existing literature there is no adequate research on the influence of different ventilation modes on a TW's performance. To this direction, this study explores three different operation modes of a classical TW, from which two are characterized by different airflow paths.

2. Methods

In the following sub-sections, the experimental setup and the adopted performance metrics are described.

2.1. Experimental setup

Three full-scale Solar Air Heating Facade (SAHF) modules were installed in an existing residential building, in Turin, northern Italy. The building consists of two floors and an attic, with a housing unit on each floor. The selected building dates from the late 18th century and it is constituted by massive vernacular masonry (mix of stone, mortar, brick, and earth).

As shown in Fig. 1, the modules are installed in the south-oriented façade on the second floor of the building. The TW modules were built in the three uninsulated wall portions between the glazing elements. The façade portion where the modules were installed is below the roof

Fig. 1. View of the building and the south-oriented façade where the modules were installed.

overhang. The modules have equal height. As Fig. 1 depicts, before the TWs' installation the external surface was painted matte black to maximize solar absorptivity. Hollow polycarbonate panels were selected to create the ventilated air cavities of the TW modules. This is a novelty compared to most studies, where single- or double-glazing elements were used. Compared to glazing systems, polycarbonate panels are lightweight and exhibit satisfying thermal transmittance values, acceptable by the European regulations [86]. Compared to traditional glazing systems with similar thermal characteristics, polycarbonate panels have lower light and higher solar transmittance [86]. In this case, though, considering that the TW modules are implemented in a real building, some key strategies were adopted to ensure better architectural integration and promote the acceptance of the elements by the building users (Fig. 2 and Fig. 3):

- The TW thickness is fully embedded by the surrounding External Insulation Composite System (ETICS) avoiding any protrusion of the TW from the façade and ensuring a clean and continuous external surface without disrupting the building's visual harmony.
- The TW height is equal to the one of the fenestrations, preserving the proportionality of the elevation.
- The TW width spans from window to window to perfectly fit the available area, reinforcing a sense of design coherence and preventing any visual fragmentation of the facade.
- A hollow multi-cavity polycarbonate creates a translucent effect, hiding the black surface of the storage wall (Fig. 3). This softens the visual impact of the system and enhances daylight diffusion, contributing to a more refined appearance.
- Minimization of the number of visible sensors in indoor and outdoor environment.
- The fan speed was also evaluated in terms of potential noise disturbance to the users.

It must be noted that by setting the TW height equal to the windows one, the upper portion of the modules ends up being shaded by the roof overhang, depending on the solar altitude. While this may reduce the overall efficiency of the modules, the choice was dictated by the architectural integration goal. The TW's cross-sections are depicted in Fig. 2, representing both the Indoor Air Curtain (IAC) and the Supply Air Façade (SAF) configurations. The first represents the classical TW

Fig. 3. View of the three full-scale TW modules.

structure where the indoor air is heated in the cavity, while the second arrangement preheats the outdoor air before entering it into the room. The inlet and outlet pipes were of a circular cross-section of 0.1 m diameter. Tables 3 and 4 present the properties of each cross-section's layer and the materials and properties of the lateral TW sides respectively.

The monitoring period lasted from November 28th, 2023, to February 28th, 2024. During this period the weather conditions and the

Table 3
Layers and properties of the TW cross-section, from the external to the internal side.

n.	Name	Thickness (m)	Thermal resistance [m^2K/W]	Solar transmittance (−)
1	Polycarbonate panel	0.016	0.48	0.6
2	Ventilated air cavity	0.08	–	–
3	Existing wall (solid brick massive wall)	0.5	0.74	–

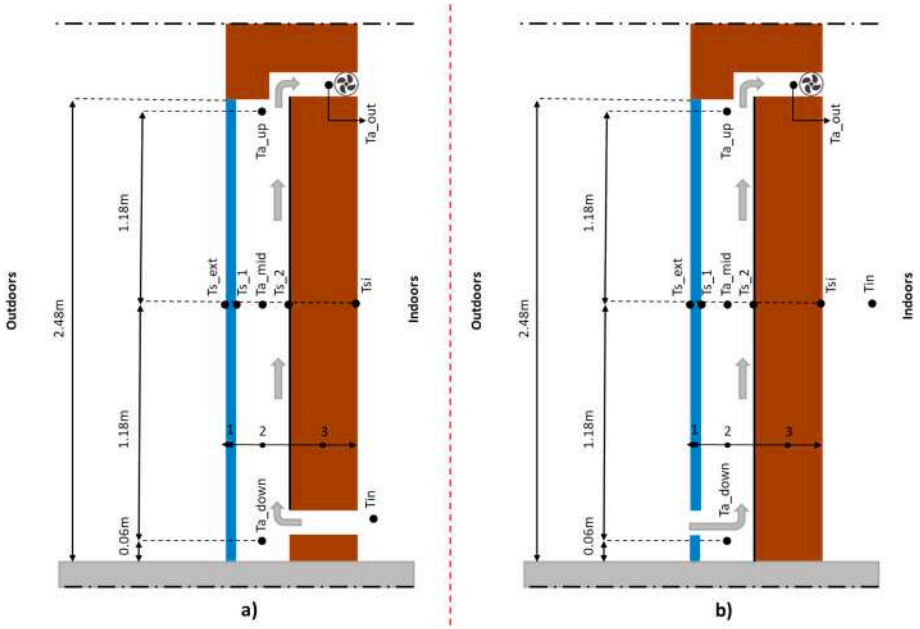

Fig. 2. TW's configurations examined and sensors placement for a) the Indoor Air Curtain mode, and b) the Supply Air Facade mode.

Table 4
Materials and thermal properties of the lateral TW sides.

Layer	Material	Thickness (m)	Thermal resistance [m^2K/W]
External	Stone	0.02	0.01
Middle	XPS	0.01	0.29
Internal	Wood	0.03	0.14

thermal performance of the walls were constantly monitored. The sensors and other devices used during the experimental campaign are presented in Table 5, with the placement of the sensors in the façade's cross-section given in Fig. 2. A datataker DT85 was also utilized to record the outdoor temperature T_{a_ext} [°C], the global horizontal $S_{ol\_h\_AV}$ [W/m^2], and the global vertical $S_{ol\_i\_AV}$ [W/m^2] solar irradiance, along with the cavity and the surface temperatures with a 15-minute timestep.

The three wall modules built in the south façade were named "Wall A", "Wall B", and "Wall C", from the right to the left (see Fig. 3). As concerns dimensions, while they have the same height, they exhibit different widths. In particular, the existing wall parts between the fenestrations, where the TW modules were installed are not equally wide, and since the researchers' intention was to fully embed the modules in the existing structure without militating unaesthetic protrusions, one of the three modules ended up with bigger area. So, Wall A and C have a width of 1.34 m, whereas Wall B has a width of 1.50 m. Another point of difference is that Wall A and C operate as IAC facades (from Dec 2nd), while Wall B in a first phase operates in Thermal Buffer (TB) mode (form Dec 2nd to Dec 16th) and in a second phase (from Dec 17th) as a SAF. In Fig. 3, the inlet of Wall B, which introduces outdoor air in the cavity during the SAF operating mode, is evidenced. For the other two walls a pipe inserts indoor air in the cavity, as depicted in Fig. 4. These pipes are also painted black to pre-heat the air before releasing it into the cavity.

In the outlet of the three walls, a fan was installed to control the ventilation rate in the cavity. The fan selected is a typical model used in air duct systems easy to be installed. An on/off rule-based control strategy was applied to manage the fans' operation with a threshold supplied air temperature for the activation set at 22 °C. In other words, whenever the air temperature on the upper part of the cavity reached or exceeded 22 °C the fan was activated, otherwise it remained off. The selection of the 22 °C threshold is reasonable considering that the typical thermostat setting in a residential building during the heating season is around 20 °C. Indeed, by applying this rule-based control strategy, the heat gains from the system's operation were secured, as outdoor air entrance during the cold nighttime hours along with the cold cloudy days was automatically excluded. This automatic control was defined to avoid the occupants' involvement, who could, however, manually deactivate the system if needed. From the vane anemometer measurements conducted, (Fig. 5), the airflow rate in Wall A, B, and C equals to 43 ± 1 m^3/h. This is a reasonable airflow rate which corresponds to about 1ach/h for a typical room size of 14 m^2 and 3 m height, avoiding excess air supply which could have a negative impact on the occupants' acoustic comfort.

While the experimental study lasted three months, a representative

Fig. 4. Inlet pipe installed in Wall A and Wall C.

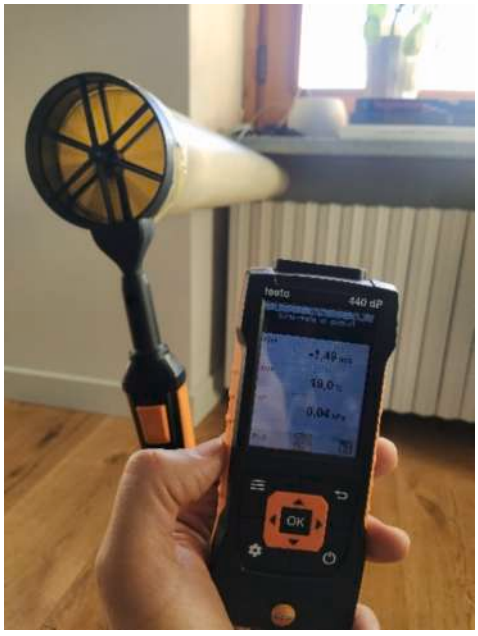

Fig. 5. Measurement of the inlet air velocity with a vane anemometer.

Table 5
Description of the sensors and devices used for the TWs' performance monitoring.

Quantity	Sensor	Accuracy	Sensor's placement
Air and surface temperatures	Type-T thermocouples	± 0.25 K	Placed in three vertical levels (low, middle, and high height) (see Fig. 2). Before installed they were calibrated. Air temperature and surface sensors were shielded from solar radiation with a plastic pipe/half pipe covered with aluminum tape.
Air velocity	Φ100mm Vane anemometer probe (Testo 440dp)	± (0.1 m/s + 1.5 % of measured value)	On the inlet of each wall
Global solar irradiance	Pyranometer (Hukseflux LP02)	Second class sensor according to ISO 9060-1990 standard. ±10 %*	On vertical and horizontal surfaces

*Uncertainty daily totals (winter, mid-latitude) [87]

week consisting of consecutive fully sunny days was identified to assess the TWs' performance during wintertime. Indeed, the most influential parameter on the systems' behavior is the global incident solar irradiance $S_{ol\_i\_AV}$ [W/m^2]. The installation of the façade modules in a residential building occupied 24 h/day introduces the imponderable factor of the occupants' behavior and choices to control indoor thermal comfort. Unlike studies conducted under laboratory conditions or in a test-cell where the indoor environment is fully controlled, in this study occupants were free to activate the radiators heating system of the adjacent rooms when the TWs were not able to guarantee comfort indoors (consecutive cloudy days), potentially altering the walls' behavior. Therefore, also this aspect was taken into consideration for the definition of the representative week, by selecting a week where the heating system was kept off to prevent it from altering the results.

2.2. Performance metrics

In an effort to assess the TWs' thermal performance, the solar efficiency parameter η_{sol} [84], was adopted. η_{sol} is the ratio of the heat supplied to the indoor environment by the pre-heated air (Q_{supply}) and the global incident solar radiation on the wall's vertical surface (Q_{sol}):

For Wall A, and C (IAC):

$$\eta_{sol_{IAC}}(\%) = \frac{\sum_n^m Q_{supply}}{\sum_n^m Q_{sol}} \bullet 100 = \frac{\sum_n^m \dot{V} \bullet C_p \bullet \rho \bullet (T_{a\_up} - T_{\_in})}{\sum_n^m S_{ol\_i\_AV} \bullet A} \bullet 100 \quad (1)$$

For Wall B (SAF):

$$\eta_{sol_{SAF}}(\%) = \frac{\sum_n^m Q_{supply}}{\sum_n^m Q_{sol}} \bullet 100 = \frac{\sum_n^m \dot{V} \bullet C_p \bullet \rho \bullet (T_{a\_up} - T_{a\_ext})}{\sum_n^m S_{ol\_i\_AV} \bullet A} \bullet 100 \quad (2)$$

where n and m declare the referenced period, $\dot{V}$ is the airflow rate in [m^3/s], C_p is the air specific heat in [J/kg K], ρ is the air density in [kg/m^3], $S_{ol\_i\_AV}$ in [Wh], T_{a_ext} the outdoor temperature in [°C], and A is the surface area of each facade. T_{a_up} was used for the calculations instead of T_{a_out}, as the goal of the study is the evaluation of the component's efficiency, and hence the heat losses attributed to the air distribution inside the indoor environment were neglected. Nevertheless, this quantity does not consider the full TW performance, as it completely neglects the thermal behavior of the massive storage wall.

To take into account also this effect, a second performance metric was defined, named total efficiency η_{tot} [88], which accounts also the heat exchange between the massive storage wall and the indoor air (Q_{cond}):

$$\eta_{tot}(\%) = \frac{\sum_n^m Q_{supply} + \sum_n^m Qcond}{\sum_n^m Q_{sol}} \bullet 100 = \frac{\sum_n^m [\dot{V} \bullet C_p \bullet \rho \bullet (T_{a_{up}} - T_{a_{ext}})] + \sum_n^m [h_i \bullet (T_{si} - T_{in}) \bullet A]}{\sum_n^m S_{ol\_i\_AV} \bullet A} \bullet 100 \quad (3)$$

where h_i is the heat transfer coefficient at the surface facing the room. This coefficient refers to the combined heat transfer through convection and radiation. Since this study is focused on the component scale, no measurements of room surface temperatures were conducted. As a result, despite the existence of empirical formulas for the calculation of the convection coefficient in isolated plates, no safe approach exists for the calculation of the radiation effect. Thus, a simplified value of 7.7 was adopted, as specified by EN ISO 6946:2017 [89]. The introduction of the total efficiency clearly indicates the two heat transfer mechanisms of the TW, from which the one is related to the supply of pre-heated air (convection) and the second to the conduction heat transfer within the massive wall which contributes to the indoor heating and occupant comfort through convection and radiation effects.

Moreover, the efficiency calculation was performed following two approaches to account for the shading effect. Indeed, the TW modules are shaded at certain hours from the roof overhang, the lateral partitions with the surrounding buildings, and the small columns on the balcony. Considering the shaded area at each timestep, two thermal efficiencies were calculated: the actual one, where all the shadings were neglected, and the amount of the incident solar radiation (as measured by the pyranometer) was equally allocated to the walls' areas, and the potential one, where the actual irradiance impinging the façade was considered, taking into account the shading and the actual sunlit area. In order to determine the actual sunlit area of each module over the entire monitoring period, the building geometry and the facing and lateral obstructions were created in SketchUp. The model was subsequently imported into EnergyPlus and the sunlit area was calculated for each timestep. Appendix provides a closer look at the shading conditions of each module.

Finally, a metric to assess the thermal buffering efficiency (η_{buf}) for the three modules had to be also considered. The index was calculated using Eq. (4) [90], considering only the hours when the ventilation system was turned off, while aiming to acquire comparable results for the three walls, the period in which Wall B operated only as a thermal buffer and its ventilation system remained constantly off was excluded from the efficiency calculation of the referenced wall.

$$\eta_{buf}(\%) = 1 - \frac{\sum_n^m (T_{in} - \overline{T_{cav}})}{\sum_n^m (T_{in} - T_{ext})} \bullet 100 \quad (4)$$

where $\overline{T_{cav}}$ equals the average value of the T_{a_down}, T_{a_mid}, and T_{a_up} variables at each timestep.

η_{buf} quantifies the TW's ability to buffer indoor temperature swings due to the outdoor temperature. Values close to 100 % mean that the cavity temperature nears the indoor one.

3. Results and discussion

This section is dedicated to the monitoring data presentation and analysis, and the evaluation of the TWs' performance. At first, there is a reference to the prevailing climatic conditions during the representative week, followed by the walls' temperatures monitored by the sensors installed. A detailed comparative analysis between both Wall A and C (IAC operation) and between the IAC and SAF modes on Walls C and B, respectively, is provided, to shed light on the complex walls' thermal behavior. The section is completed with the performance assessment of the three walls according to the metrics presented in Section 2.2.

3.1. Outdoor boundary conditions

The representative week used to assess the three TW modules' performance consists of six consecutive fully sunny days with the heating system turned off. After examining the whole period results, the period from December 14th, 2023, to December 19th, 2023, was identified. The selected days were characterized by high $S_{ol\_i\_AV}$ and relatively low outdoor temperatures, ranging from 0.5 °C to almost 15 °C. The graph depicted in Fig. 6 presents the variation of the T_{a_ext} with the blue line, and the one of the parameters $S_{ol\_h\_AV}$ (grey line) and $S_{ol\_i\_AV}$ (orange line) for the representative week. In Table 6 the lower and peak values of these three parameters are provided on a daily basis, for the representative week. The activation and deactivation time of the ventilation in the three walls are provided in Table 7.

It is worth to be mentioned here that in Turin area there are relatively low winds as the city is surrounded by the Alps, from the west and north, which usually results in calm conditions. This trend was verified by the measurements, as during the whole period wind speed remained lower than 2.5 m/s except for few single days where the speed ranged from 2.5 m/s to 4 m/s. Considering this phenomenon, and that the only configuration working in SAF mode, i.e. Wall B, operates with mechanical ventilation system, the wind effect has a negligible influence on the walls' performance.

During the representative week, no occupant interventions on the

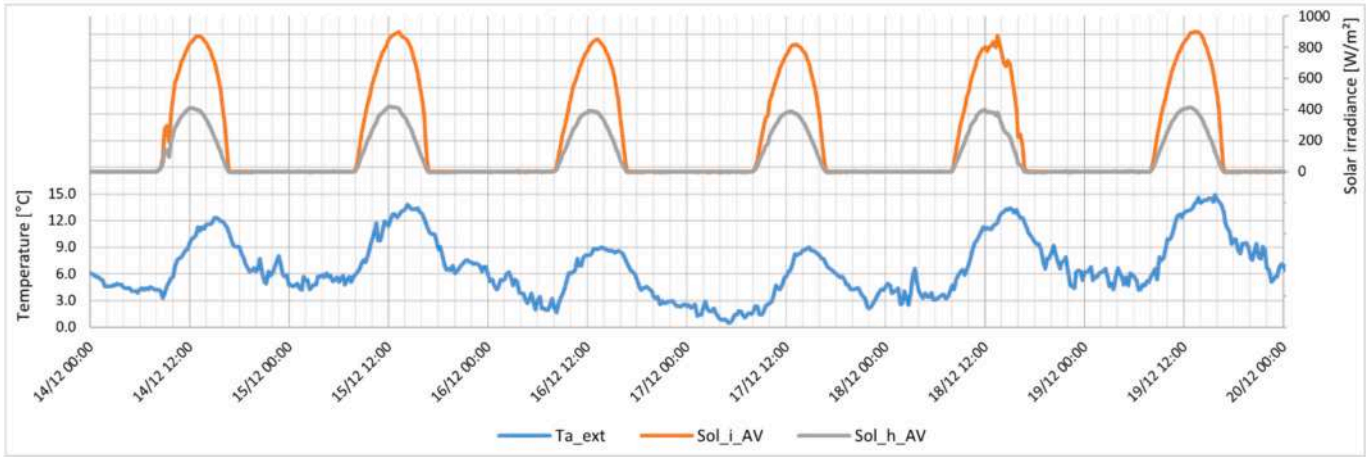

Fig. 6. Boundary conditions variation during the representative week: 14/12 to 19/12, 2023.

Table 6
Boundary conditions (daily, lower, and peak values) during the representative week: 14/12 to 19/12, 2023.

Date	Maximum T_{a_ext} [°C]	Minimum T_{a_ext} [°C]	Maximum $S_{ol\_i\_AV}$ [W/m^2]	Daily $S_{ol\_i\_AV}$ [Wh/m^2]	Maximum $S_{ol\_h\_AV}$ [W/m^2]	Daily $S_{ol\_h\_AV}$ [Wh/m^2]
14/12	12.3	3.3	872.8	4980.5	411.7	2135.5
15/12	13.8	4.2	900	5449.6	419.1	2278
16/12	9	1.7	852.1	4819.5	393.9	2073.2
17/12	9	0.5	818.6	4641.3	388.9	2041.4
18/12	13.4	2.5	874.7	4928.4	398.8	2122.9
19/12	14.9	4.2	901.3	5434.1	415.1	2254.9

Table 7
Opening and closing time of the ventilation system in Walls A, B, and C during the representative week.

Date	Fan activation time			Fan deactivation time		
	Wall A	Wall B	Wall C	Wall A	Wall B	Wall C
14/12	10:30	–	10:30	19:00	–	19:00
15/12	10:00	–	10:00	20:00	–	20:00
16/12	10:30	–	10:30	18:30	–	18:30
17/12	10:30	10:30	10:30	19:30	19:30	19:30
18/12	10:15	10:15	10:15	20:00	20:00	20:00
19/12	10:00	10:00	10:00	20:00	20:00	20:00

heating system were recorded, and the system remained off in the monitoring rooms, ensuring that the energy profile of the walls remained unaffected.

3.2. Cavity and interface temperatures

Considering that Wall A and C operate under the same principle the experimental results of these two configurations will be presented together. The temperature profile of the air in the cavity of Wall A, as recorded by the installed thermocouples, is depicted in Fig. 7, and for Wall C in Fig. 8, while Table 8 provides the average weekly maximum value of the air temperature variables both for Wall A and Wall C for the representative week. As already described in the Methods section, the thermocouples were placed in different cavity positions, subdividing the cavity into three fictional vertical subzones, providing also data from the outlet pipe (on its inlet and outlet). In the graph, the room's indoor

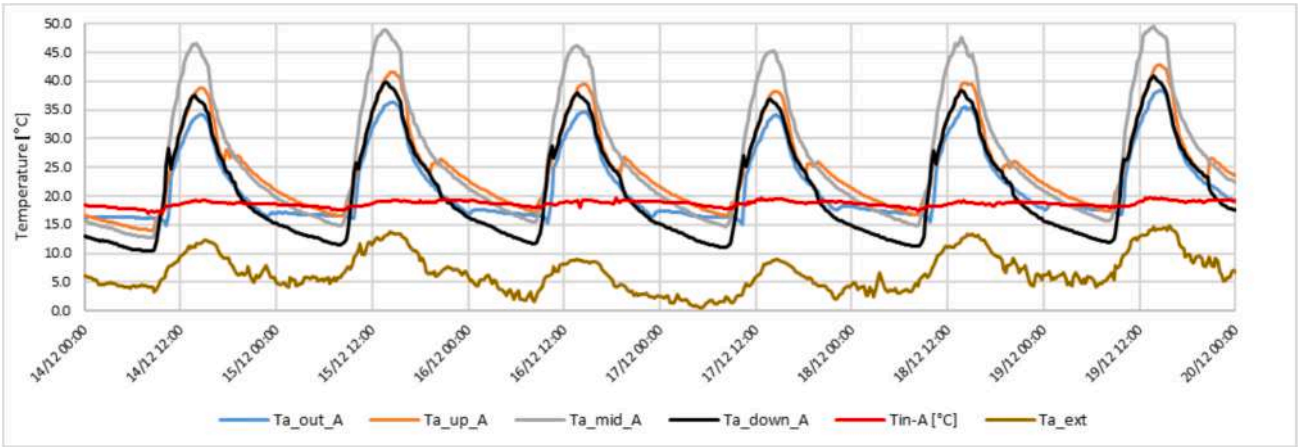

Fig. 7. Temperature profile of the ventilated cavity, the indoor and outdoor environment for Wall A during the representative week.

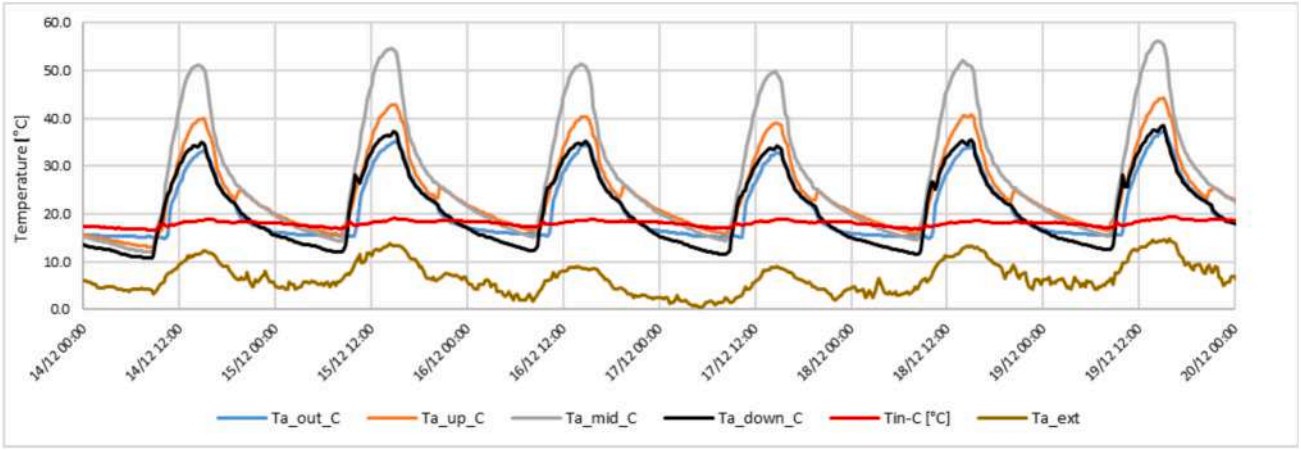

Fig. 8. Temperature profile of the ventilated cavity, the indoor and outdoor environment during the representative week for Wall C.

Table 8
Average weekly maximum air temperature variables for the representative week: 14/12 to 19/12, 2023 for Walls A and C.

Module	Weekly average max. daily Ta_out [°C]	Weekly average max. daily Ta_up [°C]	Weekly average max. daily Ta_mid [°C]	Weekly average max. daily Ta_down [°C]
Wall A	35.5	40.1	47.3	38.6
Wall C	34.6	41.3	52.6	36.0

temperature is also represented by the red line.

The indoor temperatures present a smooth profile free of sharp and intense variations, proving that no heating system was operating close to Wall A or Wall C during this week. Some small variations appearing in the indoor air could be attributed to the electric equipment operating in the room located behind Wall A, which hosts the kitchen and the dining room of the house.

The highest reached temperatures every day correspond to T_{a_mid}, and not to T_{a_up}. This is the result of the roof overhang's shading on the upper parts of the TWs, limiting these parts' insolation only to a short period in the afternoon. The maximum temperatures reached during daytime are close to 50 °C for Wall A, recorded from 13:30 to 14:15, and close to 56 °C for Wall C between 14:30 and 15:00. The higher air temperatures developed in Wall C are reasonable, since Wall A receives more shading from the adjacent building and the wider column in the balcony. Looking carefully at the graphs, starting the analysis from bottom to top of the cavity, the temperature on the bottom part of the cavity is much higher than the indoor one during daytime in both modules, which can be related to the pivotal role of the inlet pipe, preheating the indoor air while directing it to the bottom of the cavity. In the morning hours, there is also a sharp increase of T_{a_down} coinciding with the fan's activation. This occurs because the indoor air entering through the inlet pipes is warmer than the cooler air in the cavity, which has been affected by the nighttime heat losses. Considering the difference between the air temperature in the mid-façade height and the one on the top of the cavity, it is extremely high during the first hours of the fan's operation when the shading maximizes, getting lower towards the afternoon. During the maximum temperatures developed in the cavities, there is a difference of about 9 °C in Wall A, and of 11–13 °C in Wall C, with T_{a_mid} being the highest. It can be also observed that there is a time lag ranging from 15 to 30 min between the peak values of T_{a_mid} and T_{a_up}, with T_{a_mid} being the first to reach its highest value between the two. In addition, comparing T_{a_up} and T_{a_out} results, it is evident that the air reaches 4–5 °C lower in the outlet of Wall A and 6.5–8 °C in the outlet of Wall C. This can be attributed to the conduction losses from the massive wall, since the outlet pipe is embedded in it. For Wall A the losses are lower as the room behind it and subsequently the wall is warmer.

For both modules, T_{a_mid} is higher than T_{a_down} during the day, apart from the hours prior to the fan's activation when the two variables equalize. Their maximum difference is spotted between 14:15–14:30 reaching up to 9 °C for Wall A and 19 °C for Wall C. A similar pattern in the difference between T_{a_up} and T_{a_down} can be observed, with less deviations though. In fact, for both modules the maximum difference reaches 3 °C in Wall A and 8 °C in Wall C, both at 15:00.

Up to half an hour after the fan turns off a sharp increase in the value of T_{a_up} can be observed, which lasts for fifteen to thirty minutes, before it gets a decreasing trend like the rest variables, while the opposite pattern can be detected for T_{a_down}, which performs a sharp decrease a few minutes after the fan shuts down. This phenomenon can be related to the buoyancy effect starting to develop in the cavities when the systems turn into a TB mode, and the heat released from the walls whose temperatures gradually drop. The decreasing trend of T_{a_up} is similar to the rest variables, whereas T_{a_down} is decreasing more than the rest variables reaching the lowest temperature at night, while T_{a_up} keeps the highest nocturnal temperature.

Overall, inside both cavities typical buoyancy profiles are observed during the night when ventilation is off. In more detail, the temperature on the lower part of the cavities is lower than the one in the middle of the cavities (with a difference ranging from 4-5 °C for Wall A and 3–4 °C for Wall C), which is lower than the temperature on the upper part of the cavities (about 1.5–2 °C for Wall A and even less for Wall C). Apparently, ventilation affects this typical buoyancy profile during daytime, as during the first hours of its operation temperatures on the lower and upper part of the cavities equalize and follow the same increasing trend. This lasts longer in Wall A as Ta_down reaches higher values due to reduced shading. When the temperature on the lower part of the cavity starts reducing, temperature on the upper parts either continues increasing or decreases with a lower rate, but still the shading of the upper part prevents the development of a buoyancy profile in the cavity as the middle part of both facades which is unshaded develops much higher temperatures. An increase in the ventilation rate would result in reduced differences between all temperatures in the cavity, especially between the ones in the lower and upper part.

The weekly average maximum daily value for each of the air temperature variables provide a clearer overview of the two modules behavior. In Wall A higher temperatures are developed on the lower part of the cavity as it is less shaded than the relevant part of Wall C, while the rest cavity variables are higher for Wall C, since Wall A is more shaded on its middle and upper part. An interesting point is that the air reaches the room at higher temperature in Wall A than in Wall C, a phenomenon caused by the higher temperatures of the kitchen which

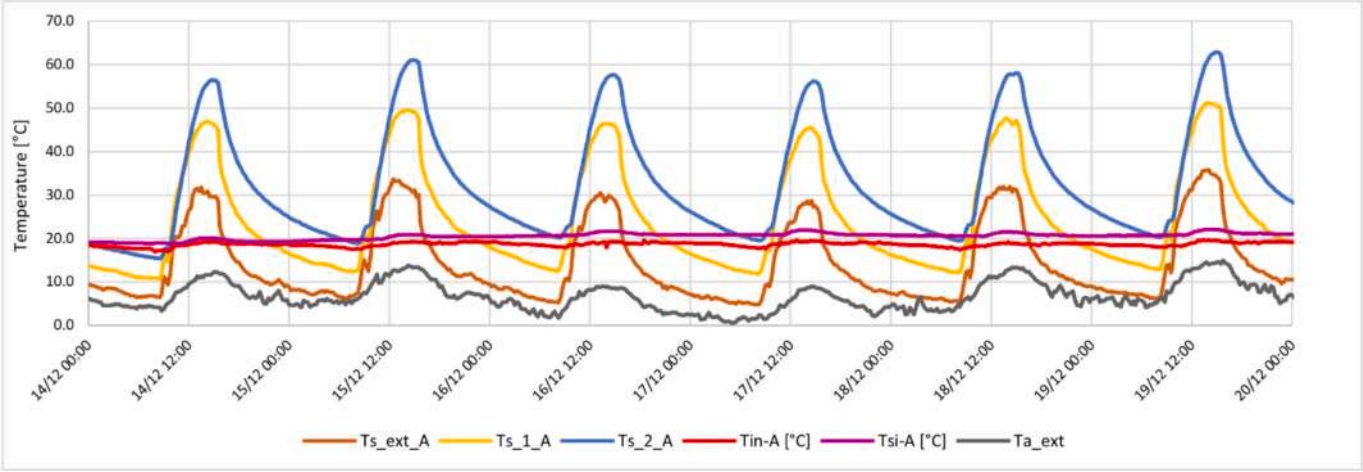

Fig. 9. Surface and outdoor temperature profiles of Wall A during the representative week.

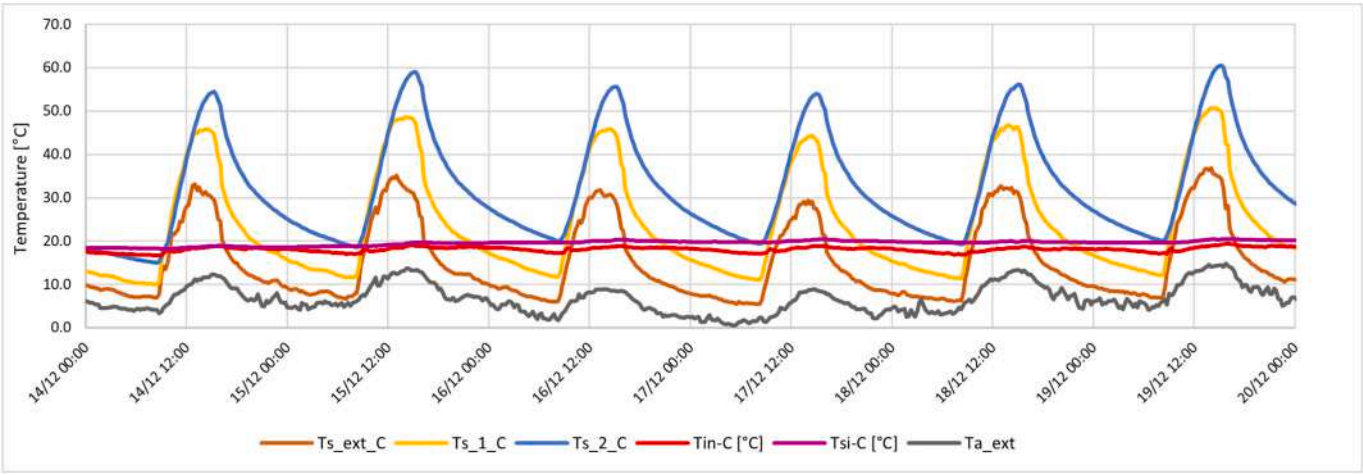

Fig. 10. Surface and outdoor temperature profiles of Wall C during the representative week.

Table 9
Average weekly maximum surface temperature variables for the representative week: 14/12 to 19/12, 2023 for Walls A and C.

Module	Weekly average max. daily Ts_ext [°C]	Weekly average max. daily Ts1 [°C]	Weekly average max. daily Ts2 [°C]	Weekly average max. daily Tin [°C]	Weekly average max. daily Tsi [°C]
Wall A	32.1	47.9	58.8	19.5	21.3
Wall C	33.2	47.0	56.7	19.0	20.0

lower the lateral heat losses from Wall A.

Fig. 9 shows the variation of the surface temperature variables along with the outdoor and indoor temperature for Wall A and Fig. 10 for Wall C, and Table 9 presents the weekly average maximum surface temperatures for the representative week. It is evident that the massive walls reach significantly high temperatures, exceeding even 60 °C in Wall A on the most sunny days (Dec 15th and Dec 19th), which corresponds to ~50 °C higher temperature compared to the outdoor one. The slightly higher Ts_2 values of Wall A stem from the elevated temperatures in the kitchen. This is also evident from the results presented in Table 9, as all the surface temperatures apart from the external temperature of the polycarbonate panel are higher in Wall A, a trend that was not present for the air temperatures. It is worth mentioning that even at night-time the walls' temperature remains close to 20 °C, while also the polycarbonate effectively maintains its internal surface temperature (T_{s_1}) over 10 °C higher than the outdoor one. Indoor surface temperature curve shows also an increasing trend, which might look limited, but considering the high thermal inertia of the wall is rather significant. For both modules, on December 14 the indoor temperature and the temperature of the wall surface facing the room are almost equal. Gradually during the week the surface temperature rises to higher values than the indoor one, which for Wall A remains stable while for Wall C it slightly increases, which indicates that the walls accumulate heat and release it indoors, considering also that the ambient temperature is always lower than the indoor one.

Moving on to Wall B, Fig. 11 provides the air temperature variables in the cavity and the indoor environment. Wall B operates in a TB mode until December 17th, when it turns into a SAF. The line representing T_{in} is stabilized between 18 °C and 19 °C during the whole week, meaning that the indoor conditions did not vary. It should be stated here that the room behind Wall B and C (dining room) was rarely occupied by the residents during the selected monitored week.

Regarding the first three days shown in the graph, when there is no ventilation and the wall operates in TB mode, the peak daytime values of the three cavity temperature variables follow a specific pattern. T_{a_mid} reaches the highest temperature, approaching 60 °C (with a peak of 63.1 °C on December 15 at 15:00), followed by T_{a_down}, while T_{a_up} remains the lowest, approximately 8 °C cooler than T_{a_mid}. Even if the natural buoyancy effect dominates in the TB mode, T_{a_up} is the lowest

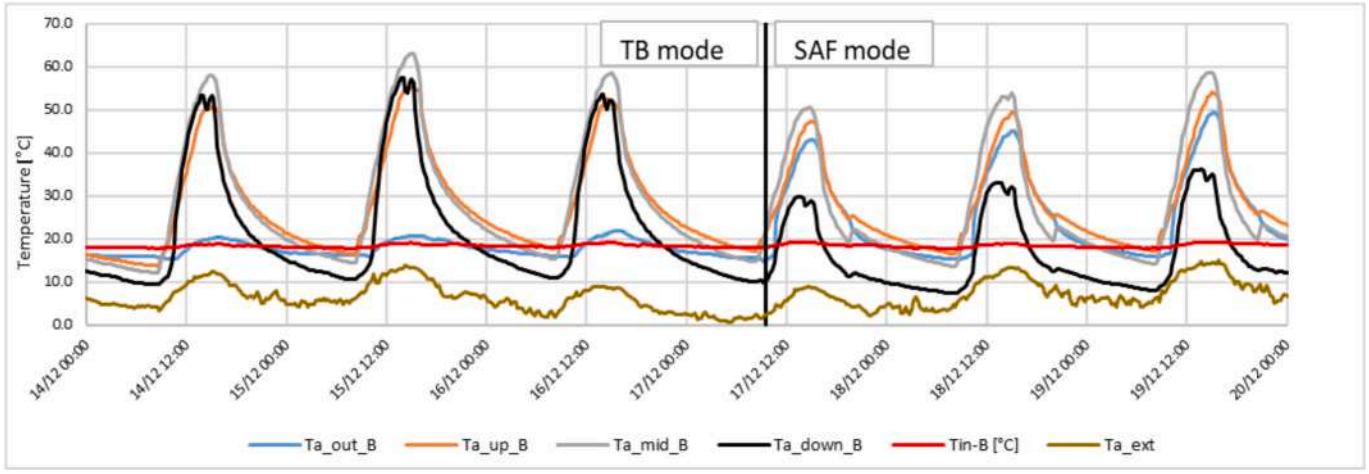

Fig. 11. Temperature profile of the ventilated cavity, the indoor and outdoor environment for Wall B during the representative week.

due to the roof's shading on the upper part of the façade. At 14:00–15:00 every day there is a sharp reduction in the bottom cavity temperature values caused by the shading of the sensors from the small balcony column. T_{a_out} remains much lower (close to the indoor temperature, nevertheless not equal to T_{in} because the outlet sensor is located in the attic) because of the lack of ventilation in the pipe. At night the variables present a typical buoyancy profile with T_{a_down} being the lowest and T_{a_up} the highest.

For the other three days Wall B operated as a SAF, so during the daytime hours that the fan operates, the temperature on the lower part of the façade presents the lowest values, then the temperature on the upper part follows and finally, the temperature in the façade's middle is the highest, with 3.5–4 °C more than the one on the upper part (reaching temperatures close to 60 °C). The temperature in the middle with the one in the lower part differs by 20 °C. Furthermore, the air entering the room reaches 4 °C to 5 °C lower than the maximum temperature reached in the façade's upper part due to the heat losses from the massive wall. The nocturnal profile of the temperatures matches the one of the TB mode, where a typical view of a buoyancy-dominated cavity can be detected.

In Fig. 12, the surface temperatures recorded by the sensors are presented for Wall B together with the outdoor temperature. Again, T_{si} variable presents an increasing trend relevant to the one recorded for Wall A, which means that the heat accumulated from the massive wall is enough to surpass its high inertia and reach its indoor side. A similar trend on the indoor temperature and the surface temperature of the wall facing the room to the one recorded for Wall A and C can be also observed for Wall B. In particular, the surface temperature gradually outnumbers the indoor one meaning that both in the TB and the SAF mode the massive wall accumulates heat releasing it to the indoor environment. The wall's surface facing the cavity (T_{s_2}) reaches very high temperatures during the afternoon which in many days exceeds 60 °C and reaches close to 70 °C for both operation modes.

No significant difference in the surface temperatures of the TB and the SAF mode was recorded. Although cavity surface temperatures on the TB mode were slightly higher than the ones recorded during the SAF mode, this difference which ranges from 2.1-9.8 °C cannot be characterized as significant if also the incident solar irradiance is considered. In particular, the minimum difference between the maximum developed T_{s_2} values for the two modes corresponds to December 15 and December 19, when the incident solar irradiance was equal to 892 W/m^2 and 901.3 W/m^2, respectively, whereas the maximum difference was detected between December 15 and December 17, with maximum solar irradiance equal to 892 W/m^2 and 815.4 W/m^2, respectively. So, the aforementioned observations indicate a low convection dissipation effect in the cavity. In other words, the façade is not fully efficient when operating under this airflow rate. To increase the convection heat transfer and consequently, the façade's solar-thermal efficiency, an increase in the airflow rate, or the implementation of fins could be also considered. The air cavity temperature profiles though, presented a more significant variation between the two ventilation modes.

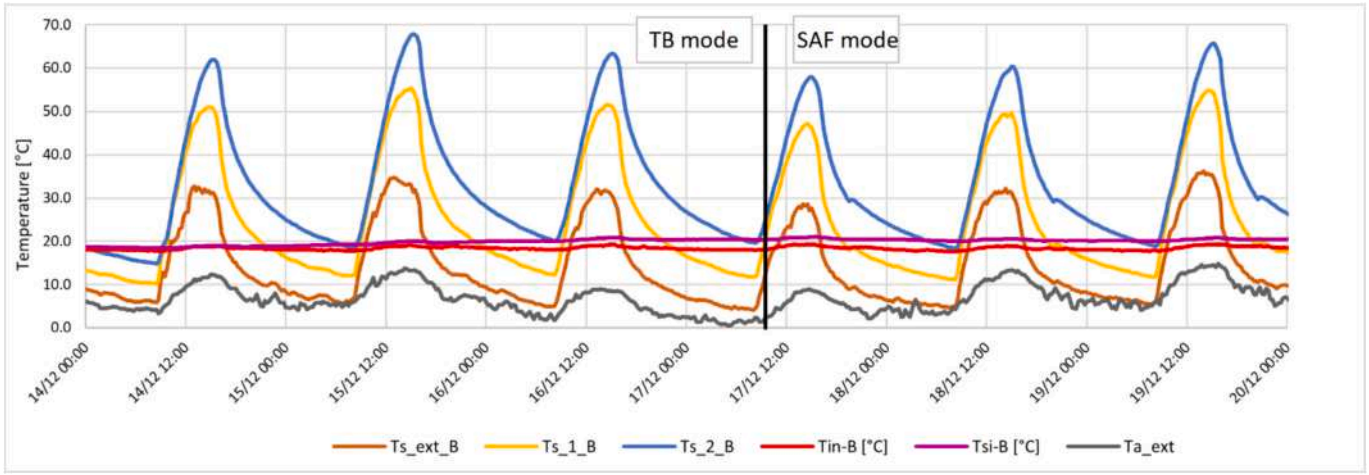

Fig. 12. Surface and outdoor temperature profiles of Wall B during the representative week.

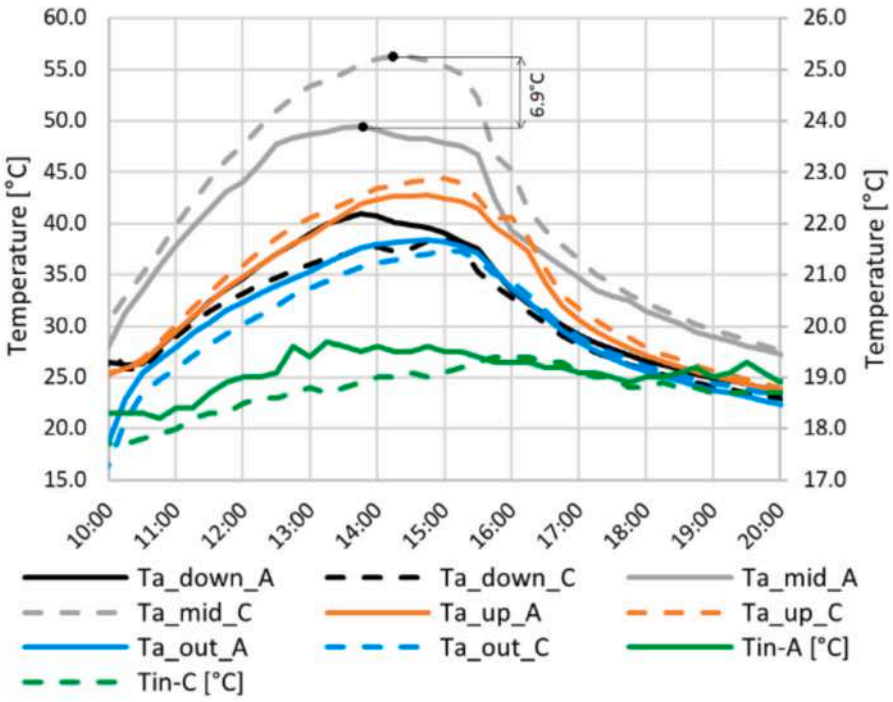

Fig. 13. Profile of the air temperature variation in the cavities of Wall A and Wall C on December 19th during the fan operation hours (refer to the left vertical axis) and the indoor temperature (refer to the right vertical axis).

3.2.1. *Comparative analysis of IAC facades behavior*

Despite the identical configurations of Wall A and Wall C, their thermal behavior presents significant discrepancies. A closer look at the variables related to the air in the cavity is depicted in Fig. 13 for the 19th of December during the active ventilation hours. The selection of this day out of the representative week was based on the maximum incident solar radiation recorded, while being the last of six consecutive sunny days ensures the absence of any temperature abnormalities within the massive wall. The data included in the graph represented by solid lines refer to Wall A, while the dashed lines refer to Wall C. A first look reveals that Wall C developed increased air temperatures in the mid and upper part of the cavity compared to Wall A, whereas Wall A presented higher temperatures on the lower part of the façade and the outlet. Starting from bottom to top, taking a closer look at the T_{a_down} profile it is observed that the mean temperature developed on Wall A during the ventilation hours is 32.2 °C and for Wall C 30.8 °C, whereas the maximum reached value for Wall A equals 41 °C recorded at 13:45, and for Wall C the highest temperature spotted in the lowest part of the façade equals 38.4 °C at 15:00. It is very important to mention that these results are related to the specific sensor's position (as presented in Fig. 2) and can be explained by the difference in the shading of each façade. In particular, the wide column located in front of Wall A shades part of the inlet pipe and the sensor of Wall C between 07:15 and 08:30, whereas Wall A receives no shading in the early morning after 07:30. During the afternoon (between 14:00–15:00) both sensors record a descending trend, which is attributed to the shading of the columns. While the shading from the column is more or less the same for both modules, the descending trend is more intense for Wall A due to the higher surface temperature it had already developed.

T_{a_mid} is the variable with the highest deviation between the two facades. Marked also in the graph, the temperature in Wall C reaches 56.3 °C, with the temperature in Wall A being lower by about 7 °C, while the mean temperatures developed during the fan's operation hours are equal to 39.2 °C and 42.5 °C for Wall A and C, respectively. This condition is the corollary of the lateral partitions and the bigger column shading on a significant portion of Wall's A area (this might not be totally clear from the solar shading graphs presented in Appendix because they correspond to specific points of the façade, while shading also affects the rest façade surfaces, e.g. the part located between the bottom and the middle, and consequently affects convection effect). On the other hand, T_{a_up} variables display similar profiles with a slight superiority of $T_{a\_up\_C}$, which is expected considering the higher temperatures developed in the central area of Wall C. Accordingly, $T_{a\_up\_A}$ reaches a maximum temperature of 42.7 °C at 14:15, while $T_{a\_up\_C}$ has a maximum value of 44.4 °C at 15:00, while the average values are 33.4 °C and 34.4 °C, respectively.

Despite the higher temperature developed on the upper part of Wall C, the air reaches warmer in the outlet of Wall A. This outcome is owed to the elevated temperature of Wall A (not the surface temperature related to the TW, but the reduced heat losses of Wall's A massive wall being in contact with the warmer dining room), which triggers lower heat losses from the air flowing in the outlet pipe. Thus, the maximum $T_{a\_out\_A}$ equals 38.4 °C at 14:45 and the maximum $T_{a\_out\_C}$ equals 37.4 °C at 15:00, whereas the mean values are 30.7 °C and 29.9 °C, respectively.

Taking into consideration the shading conditions of both modules along with the indoor conditions Wall C seems more efficient in developing high surface temperatures (excluding the lower part of the façade, where in Wall A less shading results in higher temperatures). Although the air reaches indoors in higher temperatures in Wall A, the effect of the higher surface temperatures of Wall C on the heat conduction through the wall cannot be overlooked. The efficiencies of the actual condition presented in Section 3.3 validate this statement.

3.2.2. *Comparative analysis of IAC and SAF behavior*

The comparative analysis between the IAC and the SAF modes was conducted between Wall B and Wall C, letting apart Wall A. Wall B and Wall C are both installed in two walls facing a room with limited use, with Wall B being wider than Wall C. Fig. 14 provides the profile of different temperature variables in the two walls for the hours of December 19th with the mechanical ventilation active. The solid lines correspond to Wall B, while the dashed lines to Wall C.

According to the graph, the variable with the wider deviation between the two facades is the outlet temperature, as for Wall C it is 37.4 °C at 15:00 while for Wall B it is 49.3°, about 12 °C higher. T_{a_mid} is

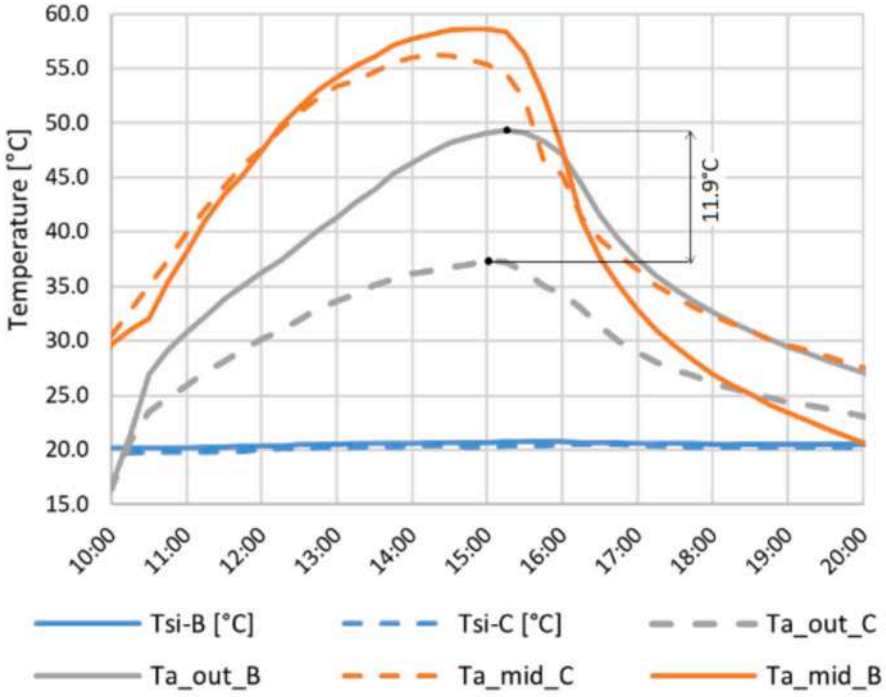

Fig. 14. Comparison of key temperature variables profile for Wall B and Wall C.

also higher in Wall B but not to the extent that T_{a_out} is, being 2.4 °C higher than the equivalent variable in Wall C. Regarding the T_{si} variable, the two walls do not present a significant differentiation, as the results in Wall B are a bit higher, but the deviation is lower than the range of 1 °C. Anyhow, Wall B appears much more effective than Wall C, which is normal considering the bigger area of Wall B and the geometry of the balcony, as Wall B is in the middle away from the lateral obstructions, receiving thus less shading.

The airflow rate provided by the fan is about 43 m^3/h for each facade. Thus, considering a 14 m^2 room with 3 m height, this airflow rate corresponds to 1ach/h provided by each TW module. Since the SAF module pre-heats ambient air, this amount of air constitutes a significant portion of the natural ventilation needed from a residential building, which in the meantime is provided in elevated temperature. This means that a SAF has dual benefits: 1) provides passive heating, and 2) neutralizes the ventilation heat losses.

3.3. Performance assessment

In this paragraph, the results of the efficiency calculations of the three walls will be provided and explained. As mentioned in the Methods section, two efficiencies were computed, named actual and potential efficiency. For the latter one, the actual sunlit area of each wall was considered for each time-step, while for the shaded areas, the influence of the diffuse radiation on the overall result was also evaluated. According to the calculations conducted, the diffuse radiation on the shaded parts of each wall can be neglected, as its effect on the efficiency is within the range of 0 % to 0.8 %.

All the results presented so far correspond to the representative week. However, the facades exhibit their highest daily performance on December 25th, a day characterized by high solar irradiance levels and outdoor temperatures exceeding 15 °C, following two consecutive sunny days. Consequently, the maximum daily η_{sol} calculations were performed for December 25th (Fig. 15). The uncertainty margins are also depicted, while the higher uncertainty of the potential metrics can be attributed to the extra uncertainty introduced by the actual sunlit area calculations from EnergyPlus. Among the facades, Wall B demonstrates

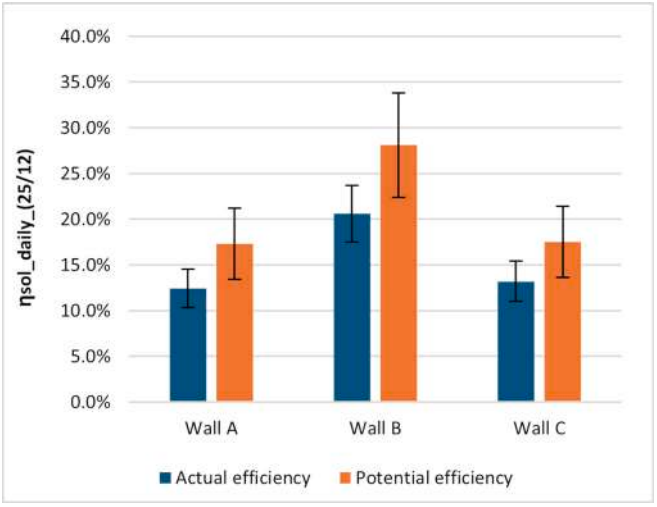

Fig. 15. Daily actual and potential efficiency η_{sol} (with the maximum uncertainty) for the three façade configurations on December 25th.

the greatest heating capacity of the circulating air due to the incident solar radiation, reaching 20.6 % when neglecting the wall's shading. Meanwhile, the actual efficiency of Wall C is approximately 1 % higher than that of Wall A. These findings are reasonable, considering that Wall B has the largest surface area out of the three and experiences the least shading from lateral obstructions. Similarly, Wall C receives less shading than Wall A, which explains its slightly higher actual efficiency.

The potential η_{sol}, which accounts for the actual incident solar irradiance, is significantly higher, particularly for Wall B, where it exceeds 28 %. Although the actual efficiency of Wall C surpasses that of Wall A, the trend evens out when considering potential efficiency. This finding highlights Wall A's superior ability to heat indoor air effectively, despite receiving more shading than Wall C. This suggests that, even though Wall C develops higher T_{a_up} values, Wall A has greater potential heating

capacity. This is primarily due to the slightly higher indoor temperature of the room adjacent to Wall A (the kitchen), which reduces heat dissipation from the solid masonry to the interior.

A direct comparison of these outcomes with relevant results from previous studies would be interesting, however, as stated in the Introduction section, no other studies examining a heavyweight TW installed on a residential building, making use of a fan-assisted ventilation exist, so a more qualitative approach will be followed here. In particular, [39] examined the performance of a heavyweight TW, installed in an unoccupied building, located in a cold region of China. The TW, operating under the IAC mode, remained active only during daytime hours, while the referenced day solar radiation intensity reached 500 W/m^2. Hourly ηsol ranged from 25-46 %. At first glance, the system examined was more effective than the one of this study, it needs to be considered though, that the indoor temperature of the unoccupied room was very low, while the massive wall had a 10 cm insulation, limiting to a significant extent the heat losses of the absorber to the indoor environment, which was not the case in the current study. Besides, the results presented on Fig. 15 provide daily ηsol values and not hourly.

Another study examined the heating performance of a concrete TW in Yazd, Iran [90]. The TW was installed in a full-scale test cell, and its solar efficiency was calculated equal to 43 % for one day in January. Compared to the 17.5 % of Wall C (potential) arising in this study, its efficiency seems double, nevertheless, the characteristics of this efficiency differ a lot. First, the experiment was conducted in a test cell and not in an occupied residential building, which means that the TW effect was more intense. Moreover, the solar irradiance of the referenced day in [91] was about 150 W/m2 higher than the one in the current study. A closer look at the experimental details reveals that the absorber developed significantly lower temperatures, while the indoor temperature of the test cell presented high fluctuation between day and night, and finally, the concrete wall had a width of 20 cm compared to the 50 cm width of the residential building's wall. Finally, the TW examined in the current study exhibits significant lateral heat losses, which cannot be quantified, but definitely reduce its performance. This means that although the two experimental cases cannot be directly compared due to the variation of the TW assemblies and the climatic conditions, a higher efficiency of a TW installed on a test cell rather than on a small part of a residential building façade was an expected phenomenon. The fact that the system implemented on an existing building presents such a high efficiency validates its potential contribution on existing and new buildings energy performance enhancement.

The efficiency metrics η_{sol}, η_{tot}, and η_{buf} were calculated for both the representative week and the entire monitoring period, except for Wall B, where results are only available seasonally due to its operation as a SAF being limited to the final three days of the representative week. The results are presented in Table 10. The weekly η_{sol} values are slightly lower than the daily ones shown in Fig. 15. Results related to Wall B demonstrate SAF's heating capacity compared to previously developed similar configurations. For instance, in [84] a lightweight TW assembly, was built and monitored in the city of Turin. The key differences with the present study was the TW's installation in a test-cell, the 24 h operation of the TW mechanical ventilation system, and the existence of a compact polycarbonate with a cellular polycarbonate panel. The experimental analysis revealed a 20 % ηsol for the month of April, which is similar to the seasonal result calculated in this study when the actual sunlit area of Wall B is considered.

Examining η_{tot}, it is evident that heat gains from the massive walls contribute to an increase of approximately 5.8 % on a weekly basis and 4.2 % on a seasonal basis compared to η_{sol} for Walls A and C. These values could potentially increase to 8.1 % and 6.6 %, respectively. A similar seasonal trend is observed for Wall B. This increase is primarily attributed to the high thermal inertia and heat capacity of the massive walls, which results in a delayed response to temperature variations within the cavity. Consequently, convection serves as the dominant heat transfer mechanism in the façade, while conduction to the indoor space further enhances the system's overall efficiency.

Walls A and C exhibit equal thermal buffering efficiency, whereas the lower efficiency of Wall B is influenced by uncontrolled outdoor air infiltration through the external vent. During the representative week, the efficiency levels of Walls A and C even exceed 100 %, as cavity temperatures remain higher than indoor room temperatures, even at night. So, a η_{buf} value higher than 100 % denotes that cavity temperature is higher than the indoor temperature in many timesteps, and that the cavity actually heats the room.

Regarding seasonal thermal buffering efficiency, it is noteworthy that Walls A and C achieve values of 94-95 %, meaning that the TW effectively neutralizes nighttime heat losses. In contrast, Wall B (SAF) shows significantly lower value of approximately 66 %, indicating that SAF experiences greater heat losses when ventilation is not active, particularly on cloudy days and during nighttime hours.

The seasonal actual efficiency is highest for Wall B, as expected, given the daily values, its larger dimensions, and reduced shading. However, the potential seasonal and weekly efficiency (considering the shading) of Walls A and C are very similar. Additionally, Wall C exhibits enhanced thermal buffering performance due to the higher temperatures developed in the cavity, as it receives less shading than Wall A, along with the slightly lower indoor temperature of the adjacent room.

Fig. 16 presents the heating energy produced from ventilation (Qsupply) and wall conduction (Qcond), along with the incident solar radiation energy on the façade and the electrical energy consumed by the fan (Efan). These are shown on both a weekly and seasonal basis for the three walls, considering either no shading (pot. Qsol) or the actual impinging irradiance (act. Qsol).

The results clearly indicate that the SAF is the most efficient system, converting approximately 15 % of the incident solar energy into heat gains for the building, considering also the fan's consumption, an amount that could increase to 22 % in the absence of shading. The performance of the IAC TW modules is similar, with Wall C being slightly more efficient due to receiving less shading. However, in the complete absence of shading, Wall A becomes almost equally efficient to Wall C due to lower heat losses to the indoor environment.

Fig. 16 confirms that convection is the dominant heat transfer mechanism in the façade, with its influence being 2–3 times greater than that of conduction. However, conduction effect should not be neglected, as for the three winter months its contribution to building's heating exceeds 37kWh for both operation modes. Finally, the electrical energy consumed by the fan accounts for less than 10 % of the thermal energy produced by Wall A and is even lower for the other two walls. This demonstrates that incorporating such a system into an existing building

Table 10
Weekly and seasonal (2/12-28/2 for Wall A and C, and 17/12-28/2 for Wall B) η_{sol}, η_{tot}, and η_{buf} calculation for the three façade configurations.

	Configuration	$\eta_{sol\_weekly\_(14/12-19/12)}$	$\eta_{sol\_seasonal}$	$\eta_{tot\_weekly\_(14/12-19/12)}$	$\eta_{tot\_seasonal}$	$\eta_{buf\_weekly\_(14/12-19/12)}$	$\eta_{buf\_seasonal}$
Actual efficiency	Wall A	10.70 %	7.40 %	16.50 %	11.60 %	100.60 %	93.50 %
	Wall B	–	11.20 %	–	15.60 %	92.80 %*	66.00 %*
	Wall C	11.40 %	8.40 %	17.10 %	12.60 %	100.80 %	95.00 %
Potential efficiency	Wall A	15.00 %	11.50 %	23.10 %	18.10 %	–	–
	Wall B	–	17.10 %	–	23.70 %	–	–
	Wall C	15.10 %	12.20 %	22.80 %	18.40 %	–	–

*The period when Wall B's ventilation system is constantly off (prior to the 17th of December) is excluded.

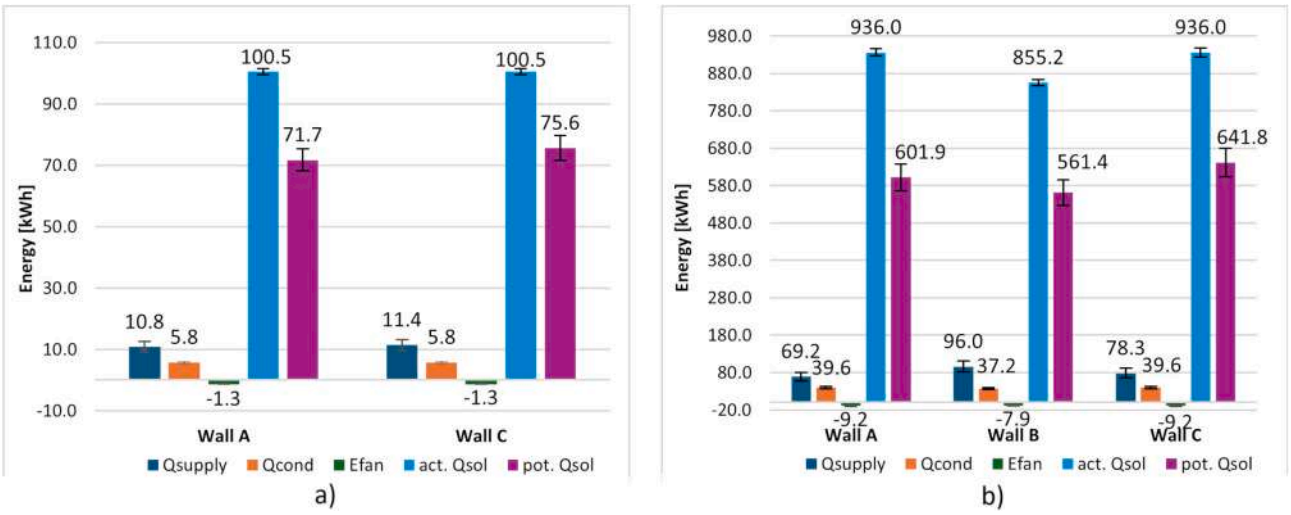

Fig. 16. Thermal energy production and electrical energy consumption (Efan) for the three facades for the actual (act. Qsol) and the potential (pot. Qsol) irradiance scenario, including their maximum uncertainties for a) the representative week and b) the whole season (Dec. 2nd to Feb. 28th for Wall A and C, Dec. 17th to Feb. 28th for Wall B).

is an effective intervention, offering significant benefits in reducing heating demand.

4. Conclusions

In this study, the performance of three full-scale architecturally integrated TW modules was assessed throughout the winter season in Turin, northern Italy. The TWs were installed on a masonry wall of a south-facing façade in an existing residential building. A fan was installed at the outlet of each wall, programmed to operate when conditions were favorable for indoor heating. Two of the walls functioned as IACs (Indoor Air Curtain mode) for the entire monitoring period, while the third initially operated as a TB (Thermal Buffer mode) before switching to a SAF (Supply Air Façade mode) for the remainder of the monitoring period. The key conclusions from the long-term monitoring analysis are as follows:

- The TWs operating as IACs under a mechanical ventilation system achieved solar efficiency over 8 % during winter, with daily efficiency reaching up to 13 %. In the absence of shading, these values increased to 12 % and 18 %, respectively. Notably, during very sunny days, the air cavity temperature in the middle section of the cavity exceeded 55 °C, with outlet temperatures approaching 40 °C.
- When evaluating TW efficiency, conductive heat transfer should not be overlooked. Heat gains due to thermal conduction through the wall accounted for over 30 % of the total gains in the IACs and about 25 % in the SAF. This contribution remained partially effective even at night and on cloudy days, as the wall continued to release stored heat, enhancing indoor thermal comfort.
- The SAF mode significantly improved wall performance. A solar efficiency of 11 % was recorded when considering only the heat gains from solar radiation in the cavity. However, when factoring in the heat released indoors by the wall's thermal mass, efficiency exceeded 15 %. The SAF module's larger wall area and reduced shading compared to the other modules likely contributed to this outcome, as both factors enhance solar radiation absorption and overall efficiency.
- The installation of a SAF in a building provides dual benefits compared to the installation of an IAC façade, as the SAF ensures passive heating while in the meantime it neutralizes the ventilation heat losses. Depending on the building type and its needs for natural ventilation a SAF can cover a significant part of them from the pre-heated ambient air supply, significantly reducing the corresponding heat losses.
- Traditional TW efficiency assessments assume uniform solar irradiance distribution across the façade. However, if only the actual sunlit area is considered (excluding shaded portions), the total efficiency, including air preheating and conductive heat gains, can reach approximately 18 % for the IAC and 24 % for the SAF during winter. Additionally, the energy consumption of the fan was minimal, corresponding to less than 10kWh per façade over the entire winter period, so the net heat gains from the TW fell within the range of 100-110kWh, depending on the façade's shading conditions for the IAC mode, and close to 125kWh for the SAF mode.

Overall, TW systems prove to be an effective solution for enhancing free solar heat gains in buildings located in temperate climates with mild to cold winters and improving occupant comfort during the heating season. The performance of these systems depends on ventilation modes, air pathways, façade area, shading, and ventilation strategy. A key parameter for the maximum efficiency of these systems is their orientation. Minimal deviations from due south ensure maximum solar exposure, and consequently maximum heat gains and optimal system performance. Moreover, incorporating a massive storage wall further optimizes TW efficiency by extending heat utilization beyond sunset, making this technology particularly well-suited for residential buildings.

Attention was also given to the architectural integration of the tested TW modules. Material selection and dimensional adaptation were carefully considered to ensure smooth integration with the existing building. This aspect is critical in real-world applications, as aesthetic compatibility plays a key role in occupant acceptance. Despite the thermal comfort benefits of TWs, their visual impact may hinder widespread adoption in practice.

The main limitations of this study are associated with the focus on the component scale. Since the monitoring period was shorter than the heating period, no data related to the building's heating system was collected, so the modules' effect on the building's heating performance was not evaluated. Moreover, the aim of this study was to examine a TW's performance when installed in an occupied building and compare different ventilation modes. No cost-benefit analysis though, was conducted for the selection of the materials used and the optimization of the fan-assisted ventilation. Furthermore, the impact of the TW's implementation on the occupants' comfort was also out of this research scope.

To this direction, future research could explore optimize the operation of the systems developed in this study, by the selection of the most

appropriate fan, the air velocity optimization, and the examination of a potential smart control systems integration to regulate the ventilation operation or the implementation of dynamic shading devices to control the TW heating performance. The optimization should not be conducted without taking the human factor into account, since apart from the TW's energy performance, its influence on the occupants' comfort (thermal, acoustic, and otherwise) is also of significant importance. Moreover, in this study the system was activated only with the scope of providing passive heat gains. Future simulation studies will be conducted to estimate the ventilation heat losses saving potential by activating the ventilation based on different ventilation activation schedules.

CRediT authorship contribution statement

Aikaterina Karanafti: Writing – review & editing, Writing – original draft, Visualization, Methodology, Investigation, Formal analysis, Data curation, Conceptualization. **Elena Badino:** Writing – review & editing, Methodology, Investigation, Formal analysis. **Valentina Serra:** Writing – review & editing, Resources, Funding acquisition, Conceptualization. **Stefano Fantucci:** Writing – review & editing, Writing – original draft, Visualization, Supervision, Resources, Methodology, Investigation, Formal analysis, Data curation, Conceptualization.

Declaration of competing interest

The authors declare that they have no known competing financial interests or personal relationships that could have appeared to influence the work reported in this paper.

Acknowledgments

The activity is part of the project NODES funded by the European Union - NextGenerationEU, Mission 4 Component 2 - ECS00000036 - CUP [E13B22000020001].

Appendix

In this Appendix the solar shading graphs for the three modules are presented. Since the shading conditions differ significantly across the height of each module, three graphs are provided for each module corresponding to the low, middle and upper measuring points.

A.1 – Wall A

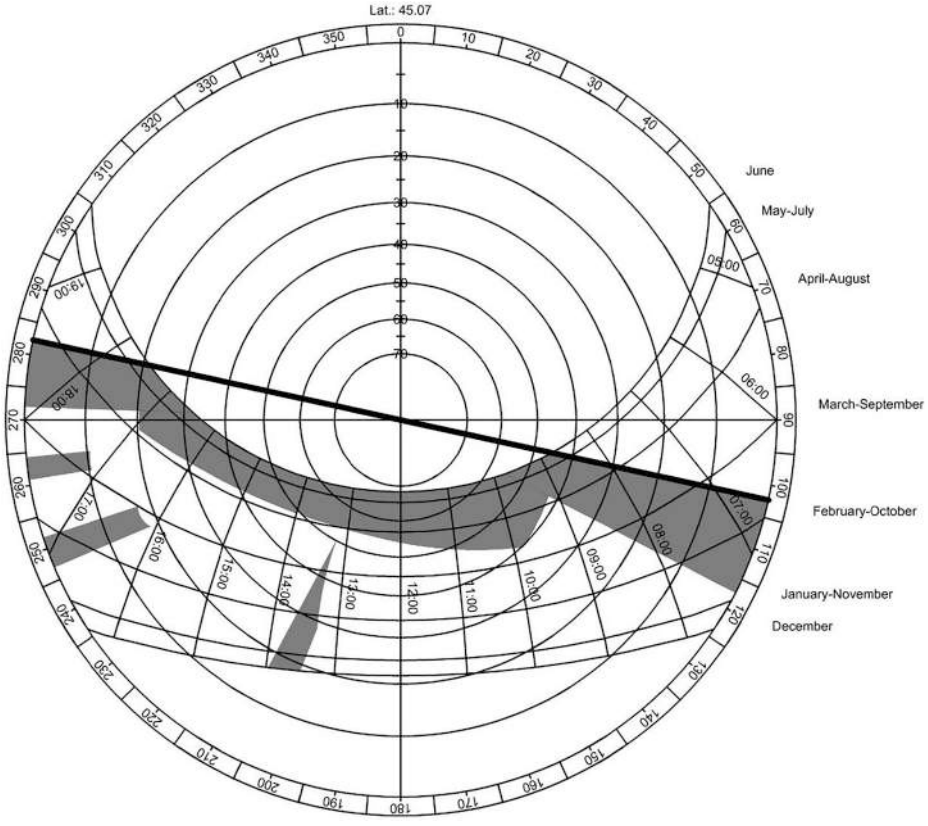

Fig. A1. Solar shading graph of the lowest part of Wall A.

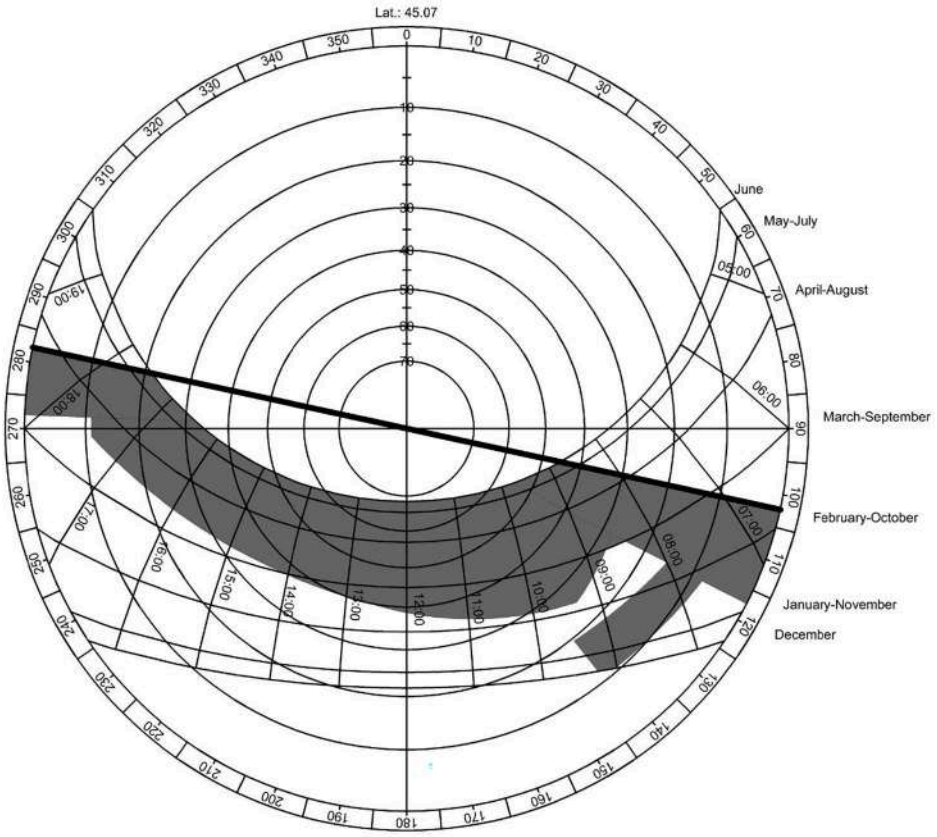

Fig. A2. Solar shading graph of the middle part of Wall A.

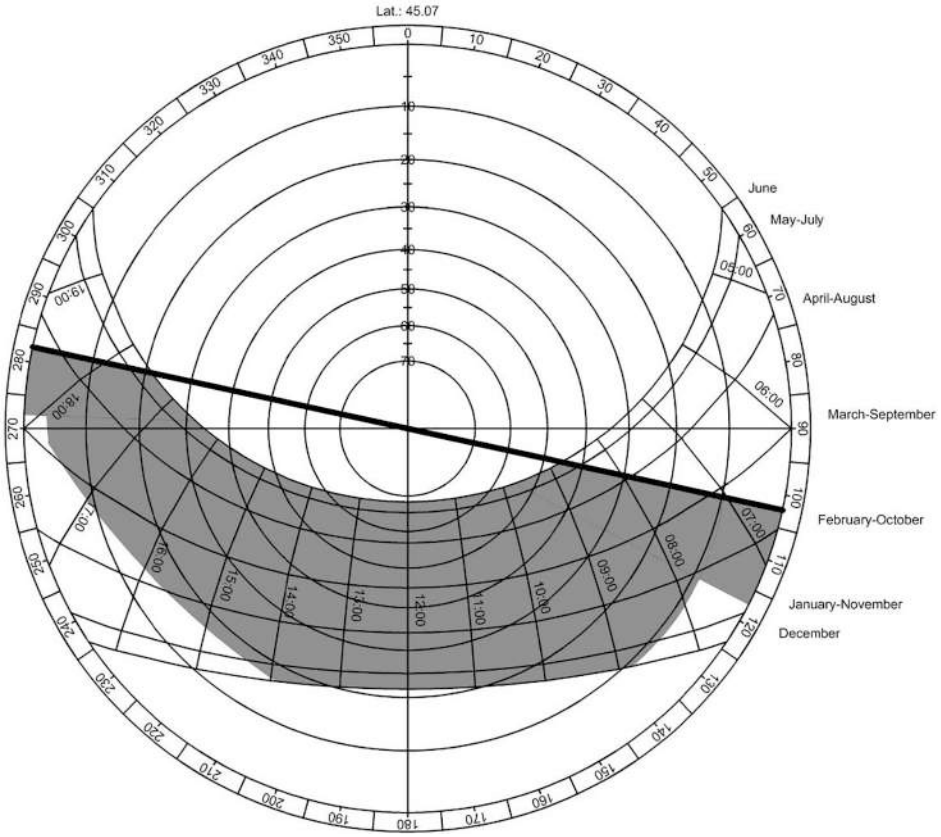

Fig. A3. Solar shading graph of the upper part of Wall A.

A2 – Wall B

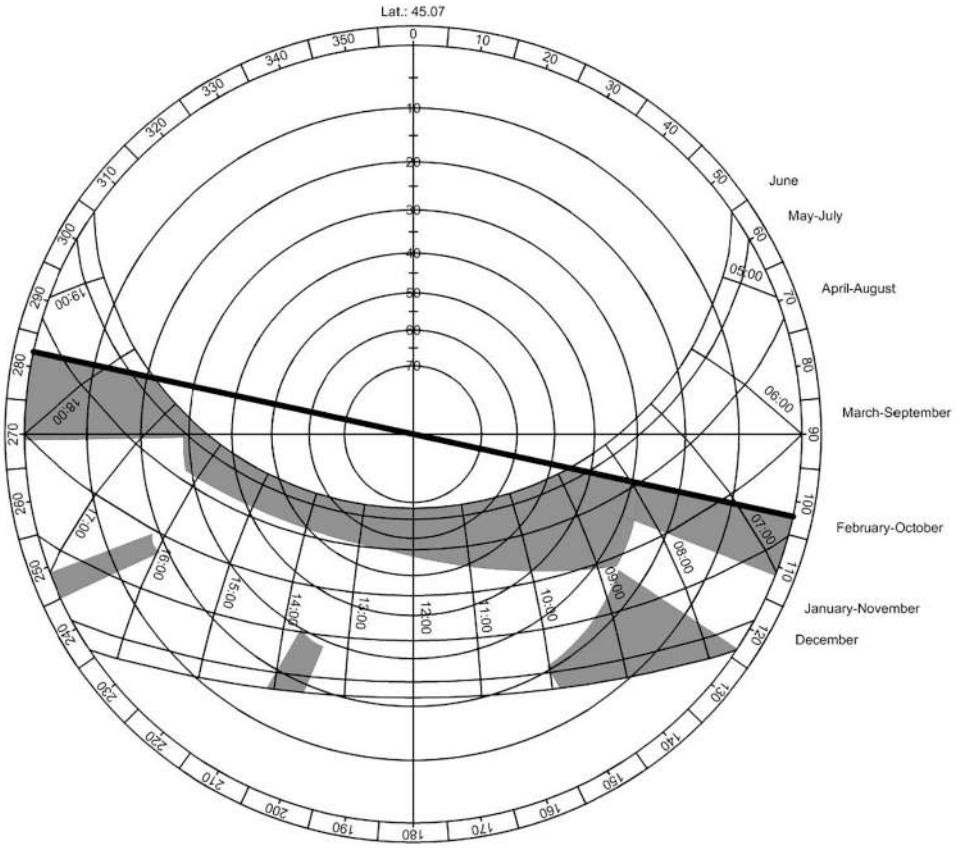

Fig. A4. Solar shading graph of the lowest part of Wall B.

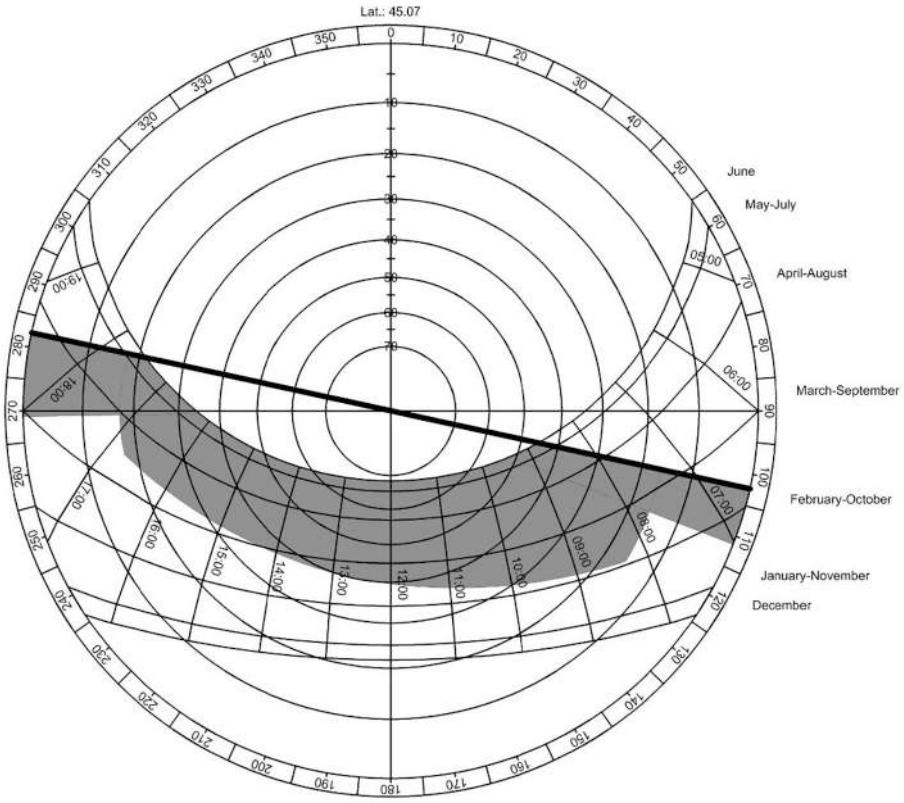

Fig. A5. Solar shading graph of the middle part of Wall B.

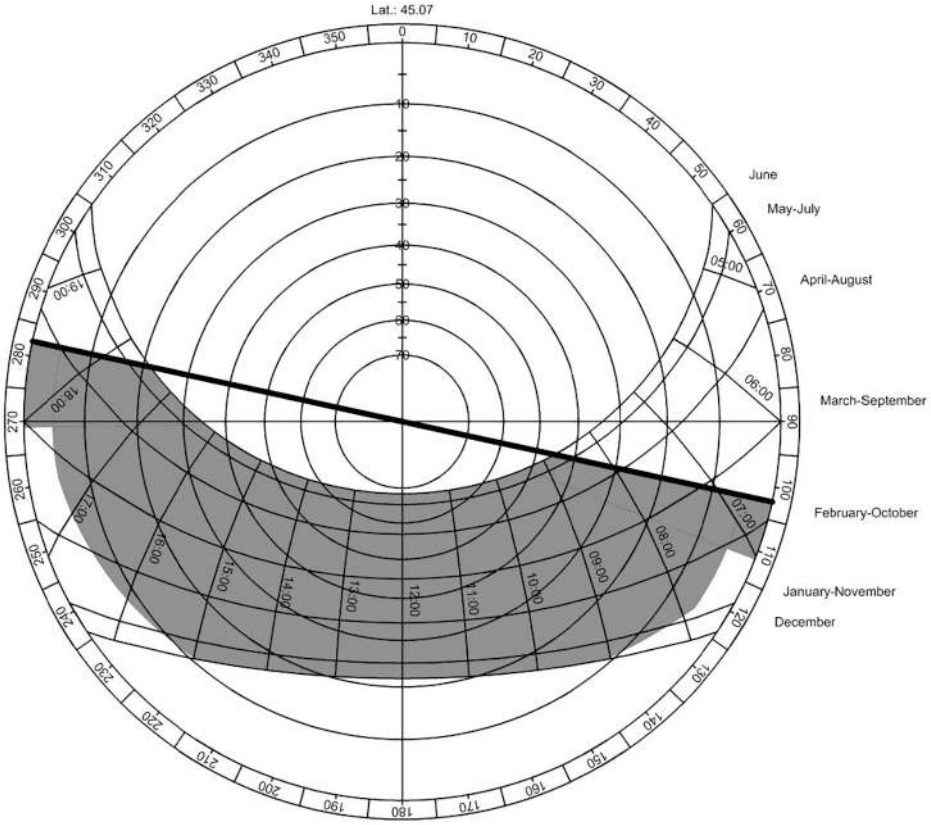

Fig. A6. Solar shading graph of the upper part of Wall B.

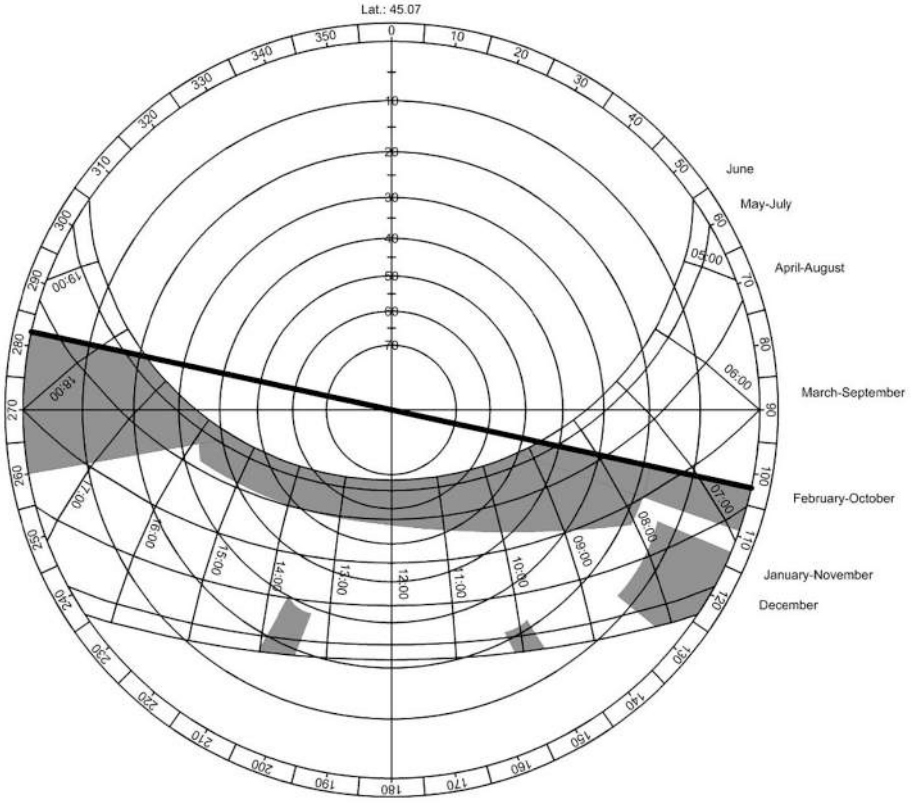

Fig. A7. Solar shading graph of the lowest part of Wall C.

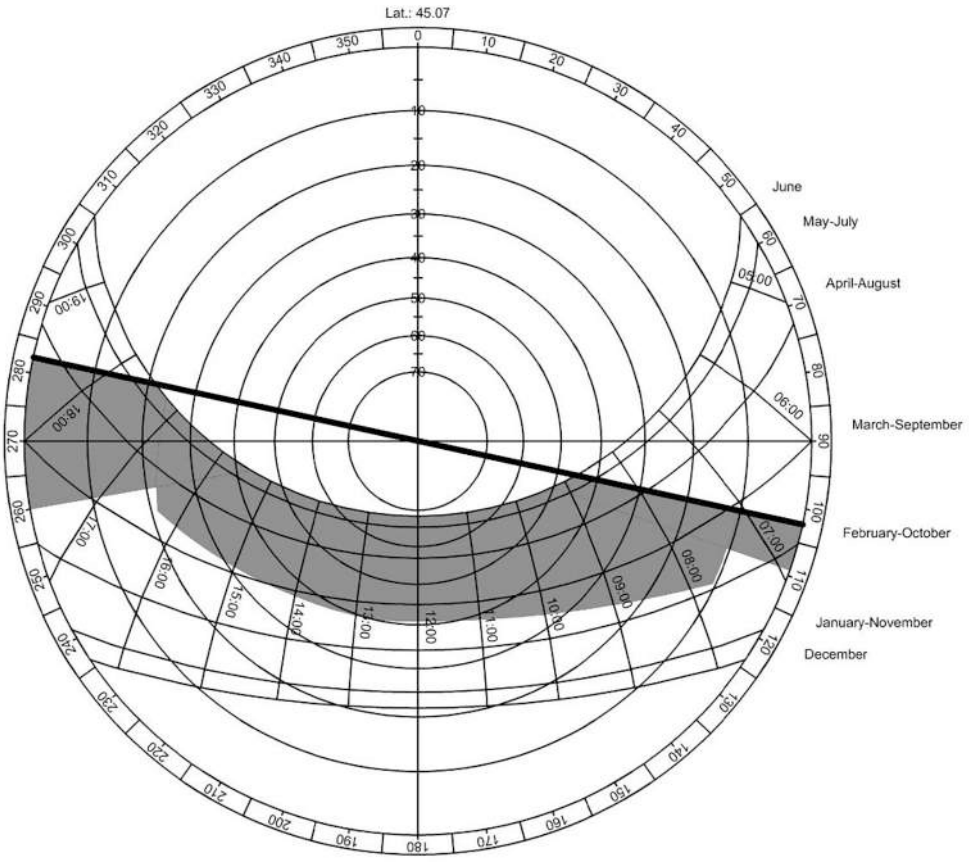

Fig. A8. Solar shading graph of the middle part of Wall C.

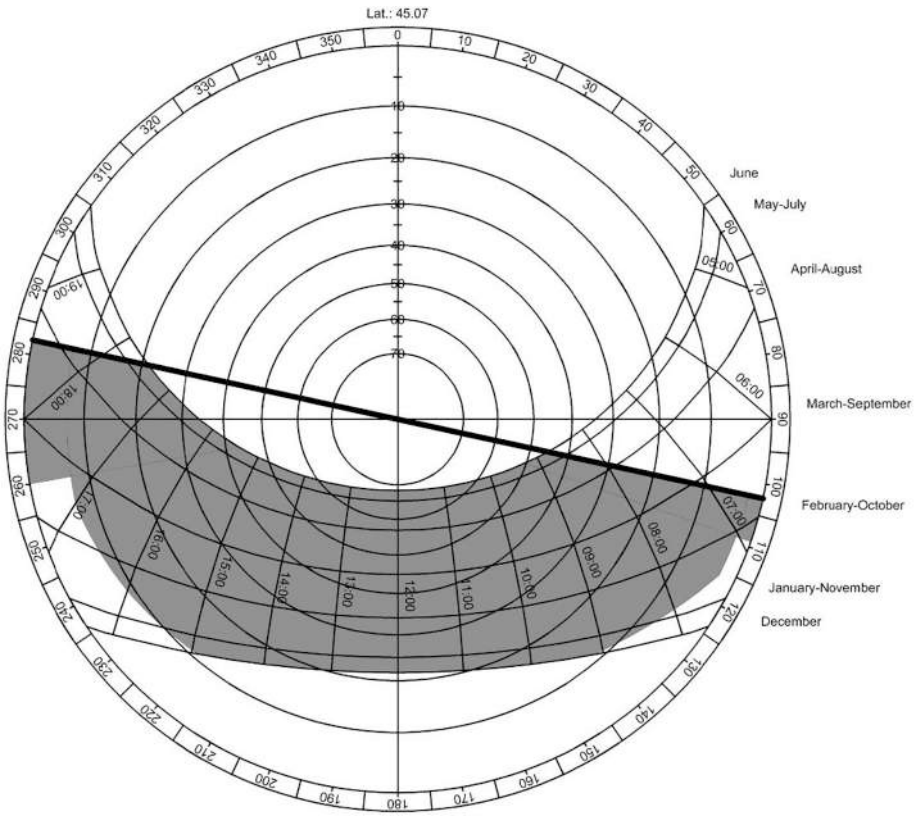

Fig. A9. Solar shading graph of the upper part of Wall C.

References

[1] International Energy Agency (IEA), Building Envelopes." [Online], Available: https://www.iea.org/energy-system/buildings/building-envelopes.

[2] A. Karanafti, T. Theodosiou, Summer thermal performance analysis of an Opaque ventilated Façade operating under the dynamic insulation principle, Energ. Build. 312 (2024) 114193, https://doi.org/10.1016/j.enbuild.2024.114193.

[3] A. Karanafti, T. Theodosiou, K. Tsikaloudaki, Assessment of buildings' dynamic thermal insulation technologies – a review, Appl. Energy 326 (2022) 119985, https://doi.org/10.1016/j.apenergy.2022.119985.

[4] K. Pelletier, C. Wood, J. Calautit, Y. Wu, The viability of double-skin façade systems in the 21st century: a systematic review and meta-analysis of the nexus of factors affecting ventilation and thermal performance, and building integration, Build. Environ. 228 (2023) 109870, https://doi.org/10.1016/j.buildenv.2022.109870.

[5] A. Tabadkani, A. Roetzel, H.X. Li, A. Tsangrassoulis, Design approaches and typologies of adaptive facades: a review, Autom. Constr. 121 (2021) 103450, https://doi.org/10.1016/j.autcon.2020.103450.

[6] A. Khanlari, A. Sözen, F. Afshari, A.D. Tuncer, Ü. Ağbulut, Z. Aytaç Yılmaz, Numerical and experimental analysis of parallel-pass forced convection solar air heating wall with different plenum and absorber configurations, Int. J. Numer. Methods Heat Fluid Flow 32 (3) (2022) 978–1001, https://doi.org/10.1108/HFF-03-2021-0160.

[7] H.-Y. Chan, S.B. Riffat, J. Zhu, Review of passive solar heating and cooling technologies, Renew. Sustain. Energy Rev. 14 (2) (2010) 781–789, https://doi.org/10.1016/j.rser.2009.10.030.

[8] O. Saadatian, K. Sopian, C.H. Lim, N. Asim, M.Y. Sulaiman, Trombe walls: a review of opportunities and challenges in research and development, Renew. Sustain. Energy Rev. 16 (8) (2012) 6340–6351, https://doi.org/10.1016/j.rser.2012.06.032.

[9] Z. Hu, W. He, J. Ji, S. Zhang, A review on the application of Trombe wall system in buildings, Renew. Sustain. Energy Rev. 70 (2017) 976–987, https://doi.org/10.1016/j.rser.2016.12.003.

[10] S.-Y. Wu, L.-F. Wu, L. Xiao, Effects of aspect ratio and inlet wind velocity on thermal characteristics of Trombe wall channel under different ventilation strategies: an indoor experiment, Exp. Therm Fluid Sci. 141 (2023), https://doi.org/10.1016/j.expthermflusci.2022.110800.

[11] K. Friji, O. Ghriss, A. Bouabidi, Y. Aryanfar, H.G. Castellanos, A. Keçebaş, Optimizing Trombe Wall performances: the impact of L-shaped fins on solar heating efficiency and building thermal comfort, Int. J. Heat Fluid Flow 110 (2024) 109658, https://doi.org/10.1016/j.ijheatfluidflow.2024.109658.

[12] S.-Y. Wu, H. Zheng, L. Xiao, Y. Xiang, Experimental investigation on the impact of fin structure factors on the finned-Trombe wall thermal performance, J. Build. Eng. 70 (2023), https://doi.org/10.1016/j.jobe.2023.106402.

[13] D. Wang, et al., Classification, experimental assessment, modeling methods and evaluation metrics of Trombe walls, Renew. Sustain. Energy Rev. 124 (2020), https://doi.org/10.1016/j.rser.2020.109772.

[14] Q. Ma, X. Wang, X. Chen, H. Fukuda, W. Gao, X. Wei, An experimental and numerical analysis of the thermal performance of double-layer Trombe walls, Energy Sources, Part A: Rec. Utilization Environ. Effects (2021), https://doi.org/10.1080/15567036.2021.1939463.

[15] Z. Hu, M. Zhu, K. Li, C. Yang, Z. Wang, W. He, Thermal performance of a novel water blind-Trombe wall system: a comparative experimental investigation, Energ. Conver. Manage. 296 (2023), https://doi.org/10.1016/j.enconman.2023.117677.

[16] H.-L. Zhang, B. Li, D.-K. Shi, W.-W. Wang, F.-Y. Zhao, Thermal performance and ventilation analysis of a zigzag Trombe wall: Full numerical and experimental investigations, Energ. Buildings 306 (2024), https://doi.org/10.1016/j.enbuild.2024.113955.

[17] H.P. Garg, Solar energy: fundamentals and applications, Tata McGraw-Hill Education, 2000.

[18] K. Sergei, C. Shen, Y. Jiang, A review of the current work potential of a trombe wall, Renew. Sustain. Energy Rev. 130 (2020), https://doi.org/10.1016/j.rser.2020.109947.

[19] M. Tunç, M. Uysal, Passive solar heating of buildings using a fluidized bed plus Trombe wall system, Appl. Energy 38 (3) (1991) 199–213, https://doi.org/10.1016/0306-2619(91)90033-T.

[20] Y. Lin, J. Ji, X. Lu, K. Luo, F. Zhou, Y. Ma, Thermal and electrical behavior of built-middle photovoltaic integrated Trombe wall: experimental and numerical study, Energy 189 (2019), https://doi.org/10.1016/j.energy.2019.116173.

[21] Y. Liu, L. Hou, Y. Yang, Y. Feng, L. Yang, Q. Gao, Effects of external insulation component on thermal performance of a Trombe wall with phase change materials, Sol. Energy 204 (2020) 115–133, https://doi.org/10.1016/j.solener.2020.04.010.

[22] S. Melero-Tur, I. Morgado-Baca, J. Neila-González, and C. Acha-Román, "Passive Evaporative Cooling by Porous Ceramic Elements integrated in a trombe wall," Passive and Low Energy Architecture (PLEA), pp. 267–272, 2011, doi: 10.5281/zenodo.10557600.

[23] T. Gu, N. Li, Y. Li, L. Che, B. Yu, H. Liu, A novel Trombe wall with photo-thermal synergistically catalytic purification blinds: material and experimental performance study, Energy 278 (2023), https://doi.org/10.1016/j.energy.2023.128013.

[24] M. Pittaluga, The electrochromic wall, Energ. Build. 66 (2013) 49–56, https://doi.org/10.1016/j.enbuild.2013.07.028.

[25] R. Gao, W. He, X. Liu, Z. Hu, H. Yu, K. Wang, The performance analysis of a novel photocatalytic-thermal-catalytic-photovoltaic-Trombe wall system integrated with compound parabolic concentrator, Build. Environ. 221 (2022), https://doi.org/10.1016/j.buildenv.2022.109301.

[26] B. Yu, X. Liu, N. Li, S. Liu, J. Ji, The performance analysis of a purified PV/T-Trombe wall based on thermal catalytic oxidation process in winter, Energ. Conver. Manage. 203 (2020), https://doi.org/10.1016/j.enconman.2019.112262.

[27] B. Yu, et al., Experimental and numerical performance analysis of a TC-Trombe wall, Appl. Energy 206 (2017) 70–82, https://doi.org/10.1016/j.apenergy.2017.08.171.

[28] W. He, Z. Hu, B. Luo, X. Hong, W. Sun, J. Ji, The thermal behavior of Trombe wall system with venetian blind: an experimental and numerical study, Energ. Build. 104 (2015) 395–404, https://doi.org/10.1016/j.enbuild.2015.06.078.

[29] W. Sun, J. Ji, C. Luo, W. He, Performance of PV-Trombe wall in winter correlated with south façade design, Appl. Energy 88 (1) (2011) 224–231, https://doi.org/10.1016/j.apenergy.2010.06.002.

[30] S.-R. Guo, et al., Experimental and numerical study on indoor thermal environment of solar Trombe walls with different air-channel thicknesses in plateau, Int. J. Therm. Sci. 193 (2023), https://doi.org/10.1016/j.ijthermalsci.2023.108469.

[31] H. Liu, Q. Tan, Y. Shi, B. Yu, M. Zhang, Enhancing indoor thermal comfort and energy efficiency: a comparative study of RC-PCM Trombe wall performance, Renew. Energy 227 (2024) 120542, https://doi.org/10.1016/j.renene.2024.120542.

[32] N. Li, et al., The experimental and numerical study on a novel all-day PCM thermal-catalytic purified Trombe wall in winter, Energy 299 (2024) 131397, https://doi.org/10.1016/j.energy.2024.131397.

[33] X. Su, et al., Experimental and theoretical analysis of photovoltaic performance and thermal behavior for bifacial PV-Trombe wall system with reversible louvers in summer, Energy 312 (2024) 133663, https://doi.org/10.1016/j.energy.2024.133663.

[34] H. Wu, Y. Li, J. Ji, N. Li, B. Yu, Field test and energy analysis on the application of thermal catalytic technology in wood buildings for contributing zero carbon buildings, Build. Environ. 268 (2025) 112334, https://doi.org/10.1016/j.buildenv.2024.112334.

[35] L. Hou, Y. Liu, T. Liu, L. Yang, Y. Feng, Q. Gao, Dynamic heat preservation at night for a Trombe wall with a built-in panel curtain in Western China, Sol. Energy 213 (2021) 284–299, https://doi.org/10.1016/j.solener.2020.10.090.

[36] C. Li, X. Yang, K. Peng, Performance study of a phase change material Trombe wall system in summer in hot and humid area of China, Energy Rep. 8 (2022) 230–236, https://doi.org/10.1016/j.egyr.2021.11.032.

[37] B. Yu, et al., The comprehensive performance analysis on a novel high-performance air-purification-sterilization type PV-Trombe wall, Renew. Energy 182 (2022) 1201–1218, https://doi.org/10.1016/j.renene.2021.11.029.

[38] H. Xie, B. Yu, J. Wang, J. Ji, A novel disinfected Trombe wall for space heating and virus inactivation: concept and performance investigation, Appl. Energy 291 (2021), https://doi.org/10.1016/j.apenergy.2021.116789.

[39] S. Hei, H. Zhang, W. Pan, A novel combined trombe wall system for village houses in cold regions of China, J. Therm. Sci. 30 (6) (2021) 2254–2266, https://doi.org/10.1007/s11630-021-1509-1.

[40] J. Long, M. Jiang, J. Lu, A. Du, Vertical temperature distribution characteristics and adjustment methods of a Trombe wall, Build. Environ. 165 (2019), https://doi.org/10.1016/j.buildenv.2019.106386.

[41] J. Long, A. Yongga, H. Sun, Thermal insulation performance of a Trombe wall combined with collector and reflection layer in hot summer and cold winter zone, Energ. Build. 171 (2018) 144–154, https://doi.org/10.1016/j.enbuild.2018.04.035.

[42] J. Dong, Z. Chen, L. Zhang, Y. Cheng, S. Sun, J. Jie, Experimental investigation on the heating performance of a novel designed trombe wall, Energy 168 (2019) 728–736, https://doi.org/10.1016/j.energy.2018.11.125.

[43] Z. Liu, D. Wu, H. Yu, W. Ma, G. Jin, Field measurement and numerical simulation of combined solar heating operation modes for domestic buildings based on the Qinghai–Tibetan plateau case, Energ. Build. 167 (2018) 312–321, https://doi.org/10.1016/j.enbuild.2018.03.016.

[44] Y. Liu, D. Wang, C. Ma, J. Liu, A numerical and experimental analysis of the air vent management and heat storage characteristics of a trombe wall, Sol. Energy 91 (2013) 1–10, https://doi.org/10.1016/j.solener.2013.01.016.

[45] N. Dimassi, L. Dehmani, Experimental heat flux analysis of a solar wall design in Tunisia, J. Build. Eng. 8 (2016) 70–80, https://doi.org/10.1016/j.jobe.2016.10.001.

[46] N. Dimassi, L. Dehmani, Performance comparison between an improved and a classical Trombe wall: an experimental study, J. Build. Phys. 40 (4) (2017) 372–395, https://doi.org/10.1177/1744259116673368.

[47] F. Abbassi, L. Dehmani, Experimental and numerical study on thermal performance of an unvented Trombe wall associated with internal thermal fins, Energ. Build. 105 (2015) 119–128, https://doi.org/10.1016/j.enbuild.2015.07.042.

[48] A. Prozuments, A. Borodinecs, D. Bajare, Trombe wall system's thermal energy output analysis at a factory building, Energies 16(4) (2023), doi: 10.3390/en16041887.

[49] B. Kundakci Koyunbaba, Z. Yilmaz, The comparison of Trombe wall systems with single glass, double glass and PV panels, Renew. Energy 45 (2012) 111–118, https://doi.org/10.1016/j.renene.2012.02.026.
[50] B.K. Koyunbaba, Z. Yilmaz, K. Ulgen, An approach for energy modeling of a building integrated photovoltaic (BIPV) Trombe wall system, Energ. Build. 67 (2013) 680–688, https://doi.org/10.1016/j.enbuild.2011.06.031.
[51] Y.A. Kara, A. Kurnuç, Performance of coupled novel triple glass and phase change material wall in the heating season: an experimental study, Sol. Energy 86 (9) (2012) 2432–2442, https://doi.org/10.1016/j.solener.2012.05.012.
[52] C. Kandilli, M. Gür, H. Yilmaz, H.F. Öztop, Experimental and numerical analyses of a model Trombe wall employing the natural zeolite/perlite composite plate as a thermal mass for nearly zero energy buildings, Int. Commun. Heat Mass Transfer 160 (2025) 108386, https://doi.org/10.1016/j.icheatmasstransfer.2024.108386.
[53] P. Miąsik, J. Krasoń, Thermal Efficiency of Trombe Wall in the South Facade of a Frame Building, 2021. doi: 10.3390/en14030580.
[54] J. Szyszka, P. Bevilacqua, R. Bruno, An innovative trombe wall for winter use: the thermo-diode trombe wall, Energies 13(9) (2020), doi: 10.3390/en13092188.
[55] A.A. Abdullah, F.S. Atallah, S. Algburi, O.K. Ahmed, Impact of a reflective mirrors on photovoltaic/trombe wall performance: experimental assessment, Results Eng. 16 (2022), https://doi.org/10.1016/j.rineng.2022.100706.
[56] A.A. Abdullah, F.S. Atallah, O.K. Ahmed, R.W. Daoud, Performance improvement of photovoltaic/Trombe wall by using phase change material: experimental assessment, J. Storage Mater. 55 (2022) 105596, https://doi.org/10.1016/j.est.2022.105596.
[57] A.A. Abdullah, F.S. Atallah, O.K. Ahmed, S. Alguburi, Effect of dusty weather on the performance of the PV/Trombe wall: experimental assessment, Case Stud. Therm. Eng. 39 (2022) 102419, https://doi.org/10.1016/j.csite.2022.102419.
[58] A.A. Abdullah, F.S. Attulla, O.K. Ahmed, S. Algburi, Effect of cooling method on the performance of PV/Trombe wall: experimental assessment, Therm. Sci. Eng. Prog. 30 (2022), https://doi.org/10.1016/j.tsep.2022.101273.
[59] O.K. Ahmed, K.I. Hamada, A.M. Salih, Performance analysis of PV/Trombe with water and air heating system: an experimental and theoretical study, Energy Sources Part A 44 (1) (2022) 2535–2555, https://doi.org/10.1080/15567036.2019.1650139.
[60] A.A. Abed, O.K. Ahmed, M.M. Weis, A.K. Ahmed, Z.H. Ali, Influence of glass cover on the characteristics of PV/trombe wall with BI-fluid cooling, Case Stud. Therm. Eng. 27 (2021), https://doi.org/10.1016/j.csite.2021.101273.
[61] A.A. Abed, O.K. Ahmed, M.M. Weis, K.I. Hamada, Performance augmentation of a PV/Trombe wall using Al2O3/Water nano-fluid: an experimental investigation, Renew. Energy 157 (2020) 515–529, https://doi.org/10.1016/j.renene.2020.05.052.
[62] Mahmud Hussain Ali, Mahmood Khalid Mawlood, Rawand Ehsan Jalal, Performance study of an isolated small scale Trombe wall with partially evacuated air gap, Adv. Mech. Eng. 16(1) (2024) 16878132231224996, doi: 10.1177/16878132231224996.
[63] M.H. Ali, M.K. Mawlood, R.E. Jalal, Investigating the impact of Trombe wall parameters on thermal performance and room temperature in the Iraqi climate, Heat Transfer 53 (5) (Jul. 2024) 2600–2635, https://doi.org/10.1002/htj.23052.
[64] M. Rabani, V. Kalantar, A.A. Dehghan, A.K. Faghih, Experimental study of the heating performance of a Trombe wall with a new design, Sol. Energy 118 (2015) 359–374, https://doi.org/10.1016/j.solener.2015.06.002.
[65] M. Rabani, M. Rabani, Heating performance enhancement of a new design trombe wall using rectangular thermal fin arrays: an experimental approach, J. Storage Mater. 24 (2019), https://doi.org/10.1016/j.est.2019.100796.
[66] A. Mokni, A. Lashin, M. Ammar, H. Mhiri, Thermal analysis of a Trombe wall in various climatic conditions: an experimental study, Sol. Energy 243 (2022) 247–263, https://doi.org/10.1016/j.solener.2022.08.011.
[67] K. Irshad, et al., Parametric analysis and optimization of a novel photovoltaic trombe wall system with venetian blinds: experimental and computational study, Case Stud. Therm. Eng. 34 (2022), https://doi.org/10.1016/j.csite.2022.101958.
[68] N. Islam, K. Irshad, M.H. Zahir, S. Islam, Numerical and experimental study on the performance of a photovoltaic Trombe wall system with venetian blinds, Energy 218 (2021), https://doi.org/10.1016/j.energy.2020.119542.
[69] C. Boulebbina, G. Mebarki, S. Rahal, Passive solar house prototype design with a new bio-based material for a semi-arid climate, Mater. Renew. Sustain. Energy 11 (1) (2022) 1–15, https://doi.org/10.1007/s40243-021-00203-y.
[70] Y. Zhu, T. Zhang, Q. Ma, H. Fukuda, Thermal performance and optimizing of composite Trombe wall with temperature-controlled DC fan in winter, Sustainability (Switzerland) 14(5) (2022), doi: 10.3390/su14053080.
[71] A. Briga-Sá, A. Paiva, J.-C. Lanzinha, J. Boaventura-Cunha, L. Fernandes, Influence of air vents management on TrombeWall temperature fluctuations: an experimental analysis under real climate conditions, Energies 14(16) (2021), doi: 10.3390/en14165043.
[72] A. Briga-Sá, J. Boaventura-Cunha, J.-C. Lanzinha, A. Paiva, Experimental and analytical approach on the Trombe wall thermal performance parameters characterization, Energ. Build. 150 (2017) 262–280, https://doi.org/10.1016/j.enbuild.2017.06.018.
[73] A. Briga Sá, J. Boaventura-Cunha, J.-C. Lanzinha, A. Paiva, An experimental analysis of the Trombe wall temperature fluctuations for high range climate conditions: influence of ventilation openings and shading devices, Energ. Build. 138 (2017) 546–558, https://doi.org/10.1016/j.enbuild.2016.12.085.
[74] V. Lohmann, P. Santos, Trombe wall thermal behavior and energy efficiency of a light steel frame compartment: experimental and numerical assessments, Energies 13(11) (2020) doi: 10.3390/en13112744.
[75] A. Martínez, C. Alonso, F. Martín-Consuegra, G. Pérez, B. Frutos, Á. Gutiérrez, Experimental analysis of a prototype for a thermochromic Trombe wall, Build. Res. Inf. 49 (7) (2021) 777–794, https://doi.org/10.1080/09613218.2021.1905502.
[76] L. Agurto, K. Allacker, A. Fissore, C. Agurto, F. De Troyer, Design and experimental study of a low-cost prefab Trombe wall to improve indoor temperatures in social housing in the Biobío region in Chile, Sol. Energy 198 (2020) 704–721, https://doi.org/10.1016/j.solener.2020.02.003.
[77] M. Dabaieh, D. Maguid, D. El Mahdy, O. Wanas, An urban living lab monitoring and post occupancy evaluation for a Trombe wall proof of concept, Sol. Energy 193 (2019) 556–567, https://doi.org/10.1016/j.solener.2019.09.088.
[78] A. Mimi Elsaid, F.A. Hashem, H.A. Mohamed, M. Salem Ahmed, Improving summer cooling in the Egypt hot/dry arid region utilizing a Trombe wall system: a field investigation, Sol. Energy 267 (2024) 112235, https://doi.org/10.1016/j.solener.2023.112235.
[79] P. Thateenaranon, M. Amornkitbamrung, J. Hirunlabh, J. Khedari, J. Waewsak, Full-scale field investigation of a bio-climatic house under Thailand tropical climate, Build. Environ. 126 (2017) 54–67, https://doi.org/10.1016/j.buildenv.2017.09.027.
[80] E. Krüger, E. Suzuki, A. Matoski, Evaluation of a Trombe wall system in a subtropical location, Energ. Build. 66 (2013) 364–372, https://doi.org/10.1016/j.enbuild.2013.07.035.
[81] L. Zalewski, A. Joulin, S. Lassue, Y. Dutil, D. Rousse, Experimental study of small-scale solar wall integrating phase change material, Sol. Energy 86 (1) (2012) 208–219, https://doi.org/10.1016/j.solener.2011.09.026.
[82] F. Stazi, A. Mastrucci, C. di Perna, Trombe wall management in summer conditions: an experimental study, Sol. Energy 86 (9) (2012) 2839–2851, https://doi.org/10.1016/j.solener.2012.06.025.
[83] F. Stazi, A. Mastrucci, C. Di Perna, The behaviour of solar walls in residential buildings with different insulation levels: an experimental and numerical study, Energ. Build. 47 (2012) 217–229, https://doi.org/10.1016/j.enbuild.2011.11.039.
[84] V. Longo, F. Isaia, S. Fantucci, L. Bianco, V. Serra, Experimental analysis on a solar air heating façade system, in: 7th International Building Physics Conference, IBPC2018, 2018, pp. 173–178.
[85] Q. Xiong, et al., Application of phase change material in improving trombe wall efficiency: an up-to-date and comprehensive overview, Energ. Build. 258 (2022), https://doi.org/10.1016/j.enbuild.2021.111824.
[86] E. Moretti, M. Zinzi, E. Belloni, Polycarbonate panels for buildings: Experimental investigation of thermal and optical performance, Energ. Build. 70 (2014) 23–35, https://doi.org/10.1016/j.enbuild.2013.11.045.
[87] Hukseflux, User manual LP02. Hukseflux Thermal Sensors, 2008.
[88] F. Isaia, S. Fantucci, V. Serra, V. Longo, The effect of airflow rate control on the performance of a fan-assisted solar air heating facade, in: IOP Conference Series: Materials Science and Engineering, vol. 609, no. 3, 2019, doi: 10.1088/1757-899X/609/3/032008.
[89] European Committee for Standardization, EN ISO 6946: Building components and building elements - Thermal resistance and thermal transmittance - Calculation methods (ISO 6946:2017). 2017.
[90] L. Rapone, G. Li Castri, M. Lavilletta, F. Favoino, M. Perino, V. Serra, Double-skin façade with air-PCM latent heat exchanger: first results from experimental campaign, Lect. Notes Civ. Eng. (2025) 436–442, https://doi.org/10.1007/978-981-97-8305-2_61.
[91] M. Rabani, Experimental comparison of energy and exergy analysis of a new designed and a Normal Trombe wall, Energy 260 (2022), https://doi.org/10.1016/j.energy.2022.125050.